JOURNAL OF PETROLOGY | VOLUME 39 | NUMBER 4 | PAGES 749–783 | 1998

Crustal Age Domains and the Evolution of the Continental Crust in the Mozambique Belt of Tanzania: Combined Sm–Nd, Rb–Sr, and Pb–Pb Isotopic Evidence

ANDREAS MÖLLER[1,2]*, KLAUS MEZGER[2]† AND VOLKER SCHENK[1]

[1]MINERALOGISCH-PETROGRAPHISCHES INSTITUT, UNIVERSITÄT KIEL, 24098 KIEL, GERMANY

[2]MAX-PLANCK-INSTITUT FÜR CHEMIE, POSTFACH 3060, 55020 MAINZ, GERMANY

RECEIVED APRIL 1, 1997; REVISED TYPESCRIPT ACCEPTED DECEMBER 3, 1997

Combination of Nd and Sr model ages and Pb isotopes on leached feldspars reveals distinct model age provinces not recognized previously within the Mozambique Belt of Tanzania. Most boundaries of these age domains are overprinted by Neoproterozoic (Pan-African) tectonism and metamorphism. Granitoids from the Archean craton show Nd model ages of 2·7–3·1 Ga and very primitive Pb isotope systematics in feldspars. Amphibolite-facies migmatites and granulites from the Mozambique Belt have similar characteristics, yet their high $^{208}Pb/^{204}Pb$ values point to U loss in the Archean, possibly during high-grade metamorphism, and subsequent Pan-African reworking. Eclogite-facies metapelites of the Early Proterozoic Usagaran Belt likewise exhibit Archean Nd model ages, but higher Pb isotopic ratios are consistent with last recrystallization of feldspar at 2 Ga. Granulites with Nd model ages from 1 to 1·5 Ga only occur in NE Tanzania; because of their restricted range in Pb isotopic composition they are interpreted as juvenile additions during late Proterozoic time. Granulites of the W Uluguru Mts have Nd model ages between 2·1 and 2·6 Ga, and highly variable feldspar Pb isotope composition indicating possible derivation from cratonic and/or Usagaran material, reworked and mixed with a small proportion of younger Proterozoic material during the Pan-African orogeny. This could indicate the suture zone between a western Archean–Proterozoic continental mass and juvenile arc-terranes docking on from the east during subduction of the Mozambique Ocean. The combined isotope data provide strong evidence that parts of the East African crust grew by lateral accretion of Early and Mid Proterozoic segments onto an Archean nucleus. However, the Neoproterozoic (Pan-African) orogeny not only led to addition of new crust in the NE of Tanzania, but also reworked older crustal material in most other parts of the Mozambique Belt. This juxtaposition of ancient with juvenile crustal segments is consistent with an active continental margin setting before or during orogenesis. Correlation with adjacent terranes indicates similar processes of mixing and limited juvenile addition prevailing throughout central Gondwana during the Pan-African orogeny.

KEY WORDS: *age province boundaries; crustal evolution; model ages; Mozambique Belt; Sr–Nd–Pb isotopes*

INTRODUCTION

The study of ancient high-grade gneiss belts provides important insights into the dynamics of deep-seated orogenic processes that often cannot be observed in modern active orogenic belts because most of these expose only the upper brittle parts of the continental crust. In such old and eroded belts, Pb and Nd isotopes supply particularly valuable information on crustal genesis, evolution and terrane amalgamation and can be used to distinguish between old reworked and juvenile crust.

This study combines Nd and Sr isotope systematics of whole rocks and Pb isotopes from leached feldspars to investigate the assembly and crustal history of the Proterozoic, polymetamorphic Mozambique Belt. The different chemical properties of the elements determine

*Corresponding author. Present address: Department of Applied Geology, University of New South Wales, Sydney, 2052 N.S.W., Australia. Telephone: 61 2 9385 5725. Fax: 61 2 9385 5935. e-mail: a.moeller@unsw.edu.au

†Present address: Institut für Mineralogie, Universität Münster, Corrensstr. 24, 48149 Münster, Germany.

their different behavior in crust and mantle processes, so that the combination of these isotope systems provides insights that prove most valuable in high-grade and polymetamorphic terranes, where substantial information is lost during later metamorphism.

Major fractionation between Sm and Nd occurs during melt extraction from the mantle. Processes in the crust including partial melting and high-grade metamorphism usually have only a minor effect on Sm/Nd systematics, which makes the Sm–Nd system ideally suited for the determination of model mantle extraction ages (DePaolo, 1988).

The Rb–Sr isotope system is less suited to obtain model mantle extraction ages because major changes in the Rb/Sr ratio can also occur in the crust by magmatic differentiation, metamorphism, weathering and sedimentary processes. As a result of these processes possibly affecting the Rb/Sr ratio of a rock, interpretation of the Sr isotope systematics of polymetamorphic rocks is often problematic.

In contrast to the Sm–Nd system, changes in Th/Pb and U/Pb occur mostly during crustal processes such as metamorphism, hydrothermal alteration, sedimentation and weathering, as a result of the different solubilities of U, Th and Pb in crustal fluids (Faure, 1986). The U–Pb system alone also preserves information on the time of parent/daughter fractionation within the crust. Minerals with very low U and Th, but high Pb content (e.g. galena) preserve the Pb isotopic composition during growth. Feldspars have also very low U/Pb and Th/Pb, but are far more abundant than galena and provide an estimate of Pb isotope composition of the whole rock during its last equilibration. Leaching ensures that only Pb incorporated during growth and not added by *in situ* decay of traces of U and Th and by Pb deposited in cracks and grain boundaries (Ludwig & Silver, 1977; Tilton *et al.*, 1981; Mezger *et al.*, 1989) is analyzed.

The use of Pb isotope systematics from leached feldspars in combination with Sm–Nd systematics overcomes a well-known ambiguity of Nd model ages where mixing of old and young material leads to intermediate Nd model ages (Arndt & Goldstein, 1987), and it is often not possible without such additional information to recognize that mixing has occurred (DeWolf & Mezger, 1994).

GEOLOGICAL SETTING

The Mozambique Belt is a major orogenic belt along the east coast of Africa. It stretches from the south of Mozambique to Sudan and Ethiopia and thus is similar in scale to modern mountain belts such as the Andes or the Himalayas (Fig. 1). Holmes (1951) defined the Mozambique Belt on the basis of the discontinuity of structural trends between the Tanzania Craton and its eastern hinterland. These roughly N–S trending high-grade gneisses east of the craton were traced by Holmes (1951) from Mozambique northwards through Tanzania into the northernmost areas of Kenya and Uganda, and were interpreted to be younger than the craton. Holmes (1951) provisionally dated the Mozambique Belt at ~1300 Ma, but it was later found that the belt was strongly affected by the 'Pan-African thermo-tectonic episode' defined by Kennedy (1964). Shackleton (1967) proposed that the Mozambique Belt extends further north into Ethiopia, and that it has a complex history. Shackleton (1967) also proposed that the Mozambique Belt comprises Archean basement and several younger metasedimentary sequences.

Rb–Sr whole-rock dating has previously been the main source of age information in Tanzania and Kenya (e.g. Wendt *et al.*, 1972; Gabert, 1973; Gabert & Wendt, 1974; Priem *et al.*, 1979; Bell & Dodson, 1981), which refined the concept of Holmes (1951) for the Precambrian geology of Tanzania and delineated absolute ages for rock formation and metamorphism. Three cycles of metamorphism were derived from this database and partly later refined by U–Pb data. An Archean event affected the craton at ~2550 Ma (Bell & Dodson, 1981), an Early Proterozoic event older than 1900 Ma affected the Ubendian (Lenoir *et al.*, 1994) and Usagaran domains (Möller *et al.*, 1995) (framing the craton in the west and the east respectively; for Usagaran see Fig. 1), and a Neoproterozoic (Pan-African) event influenced the whole Mozambique Belt, including to some extent the Usagaran belt (Möller *et al.*, 1995). The age of the Pan-African metamorphic event in Tanzania has now been dated at 615–650 Ma on the basis of U–Pb monazite geochronology from granulites in the Mozambique Belt (Möller *et al.*, 1994; Möller, 1995), consistent with some U–Pb zircon data obtained previously (Coolen *et al.*, 1982; Maboko *et al.*, 1985; Muhongo & Lenoir, 1994). Age differences of about 10–15 my occur between the different granulite mountain ranges studied in this paper. For the purpose of this study it is sufficient to take the upper age limit for Pan-African high-grade metamorphism in eastern Tanzania at 650 Ma.

The interpretation of the nature of the Mozambique Belt has led to an important controversy between plate tectonics (Burke *et al.*, 1977), vertical tectonics (Watson, 1976), and ensialic origin (Kröner, 1977). Early on it was thought that the Pan-African metamorphic event had just reworked previously existing (Archean) crust (Watson, 1976; Kröner, 1977). This view was challenged by Burke *et al.* (1977), who interpreted the Mozambique Belt as one of the prime examples of collisional belts formed by plate tectonic processes, which involves the formation of new crustal material in a standard Wilson cycle (e.g. Miyashiro *et al.*, 1984). Paleomagnetic evidence also suggests that a 'Mozambique Ocean' was once present

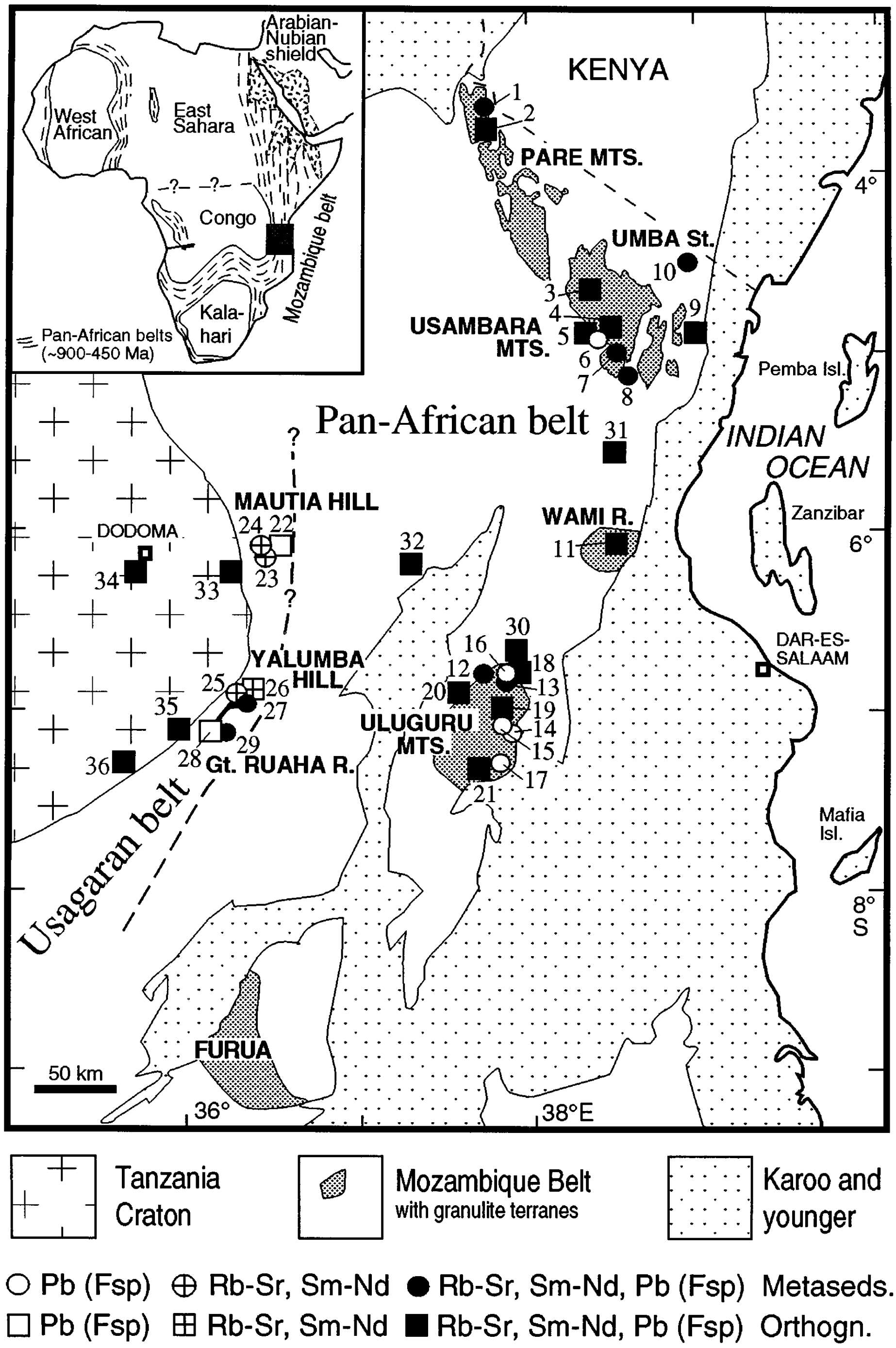

Fig. 1. Simplified geological map of eastern Tanzania. Modified from Coolen (1980), after the geological map of Tanzania (Quennell, 1960). Newly recognized granulite occurrences in the Mozambique Belt after Appel *et al.* (1998). The western limit of Pan-African metamorphic influence on the Usagaran Belt is indicated by a dashed line after Gabert (1973) and Priem *et al.* (1979). Numbers show sample locations (Nd and Sr whole-rock isotopes and Pb isotope composition of leached feldspars).

but the oceanic crust was consumed during the collision of East and West Gondwana (Meert *et al.*, 1995; Meert & van der Voo, 1996). Outlining the rival tectonic concepts stresses the importance of the recognition of crust-formation events for multiply metamorphosed orogenic belts in general, and for the Mozambique Belt of Tanzania in particular.

Stern (1994) proposed the use of the term 'East African orogen' for the areas covered by the older terms 'Arabian–Nubian shield' and 'Mozambique Belt' in East Africa because he argued that it is appropriate to view the whole area as the product of a single, Pan-African, Wilson cycle. Stern (1994) suggested that the two areas belong to the same orogenic belt and that their respective characteristics are expressions of plate-tectonic processes in different geotectonic settings of the same orogen. The Arabian–Nubian shield contains large tracts of newly formed crust and abundant ophiolites, and is interpreted (Stern, 1994) as a collage of accreted terranes, whereas the Mozambique Belt (MB) with its high-grade gneisses resembles the deeply eroded root of the orogen that experienced further uplift during rifting in the Phanerozoic and was more affected by uplift related to the formation of the East African Rift.

Of special interest are ages of crust formation and their relation to the assembly of the crust of East Africa and Gondwana. Assumptions on the regional extent of the rejuvenated versus the juvenile part of the MB have largely been based on lithostratigraphy, structures or metamorphic grade (Key *et al.*, 1989; Muhongo, 1991; Pinna *et al.*, 1993). Isotope data on the amount and distribution of crust added to pre-existing Archean material within the Mozambique Belt are scarce. Some U–Pb zircon data on the granulites showed evidence for either Proterozoic (Maboko *et al.*, 1985) or Archean (Coolen *et al.*, 1982) precursors.

A subdivision of the Mozambique Belt into a Neoproterozoic (Pan-African) metamorphic domain to the east and an Usagaran (= Ubendian, Early Proterozoic) metamorphic domain to the west is based on Rb/Sr biotite ages. Progressive increase of the mineral ages towards the west was interpreted as representing the western limit of the Pan-African metamorphic overprint on the older event (Wendt *et al.*, 1972; Gabert, 1973; Priem *et al.*, 1979). This metamorphic front runs in a SW–NE direction and closely approaches the craton on its eastern flank (Fig. 1). However, this subdivision does not *a priori* indicate the extent of these crustal domains before the orogenic cycles or the age domains within the Mozambique Belt.

The best exposures in the Mozambique Belt of eastern Tanzania are the granulite complexes, some of which are interpreted as fault-bounded mountain ranges (Bagnall, 1963; Bagnall *et al.*, 1963; Sampson & Wright, 1964). These complexes exhibit striking similarities in lithology, structure and grade of metamorphism (Coolen, 1980; Appel *et al.*, 1998).

Our set from Tanzania comprises samples from a belt of eclogite-facies rocks close to the Archean craton; from the Archean craton; from the granulite complexes formed by the Pare Mts, Usambara Mts, Umba Steppe and the Uluguru Mts; and from some lowland migmatite and granulite exposures between the mountainous granulite complexes (Fig. 1). Each of these areas may have a distinct geodynamic history, which this study aims to resolve with the combined Nd, Sr and Pb isotope systematics of their rocks. As discussed above, it is the combination of the isotopic data that should improve greatly data interpretation in terms of true crust formation and possible metamorphic or other influences. Typical rock types were chosen and comprise mostly enderbitic but also charnockitic to gabbroic orthogneisses from the granulite-facies complexes, eclogite from the eclogite-facies complex in the Usagaran Mts and granitoids as well as granitoid gneisses from the Archean craton. Where available, metapelites complete the sample set as indicators for crustal provenance.

RESULTS

The Sm–Nd and Rb–Sr data are listed in Table 1 and include duplicates for dissolution and mass-spectrometer analyses. Major and trace element analyses, including rare earth elements (REE), by X-ray fluorescence (XRF) and inductively coupled plasma mass spectrometry (ICP-MS) for all these samples have been reported by Appel (1996). A table with descriptions of sample locations and the mineral assemblages is available on request from the first author.

Nd and Sr evolution of the depleted mantle and parent/daughter ratios

Various models have been proposed for the evolution of the depleted mantle (e.g. DePaolo, 1981; Goldstein *et al.*, 1984; Liew & Hofmann, 1988). For the discussion here, the model proposed by Goldstein *et al.* (1984) was selected. This model assumes a linear evolution of $^{143}Nd/^{144}Nd$ in the depleted mantle from a 4·6 Ga deviation from CHUR to a modern ε_{Nd} value of approximately +10 (Fig. 2), and is based on the highest ε_{Nd} value of young mantle-derived rocks. These values represent the most likely depleted mantle composition, because crustal contamination would lower the $^{143}Nd/^{144}Nd$ values significantly (Goldstein *et al.*, 1984). Choice of any other model would not alter the conclusions of this paper, because throughout the age-range of the Tanzanian samples, the difference of Nd model ages calculated from

Table 1: Sm–Nd and Rb–Sr whole-rock isotope data

Fig. 1 no.	Sample no.	Rock type	Sm (ppm)	Nd (ppm)	^{147}Sm/^{144}Nd	^{143}Nd/^{144}Nd	ε_{Nd} T_0	T_{DM}G[1] (Ga)	Corr. T_{DM}G[1]	Rb (ppm)	Sr (ppm)	^{87}Rb/^{86}Sr	^{87}Sr/^{86}Sr	*T*Sr DM[2] (Ga)	Corr. *T*Sr DM	Sr initial	at T (Ga)	ε_{Sr} initial
Pare Mts																		
1	**A16G**	metapelite	3·97	14·90	**0·1612**	0·512651±5	0·3	**1·5**	1·1	43	217	0·574	0·709251±7	0·96		0·704	0·65	2·9
2	**A26-2**	calcsilicate	2·81	11·74	0·1447	0·512573±3	−1·3	**1·3**		0·5	407	**0·004**	0·703951±7	neg.	1·1	0·704	0·65	2·6
Usambara Mts																		
3	**T121G**	charnockite	2·36	11·53	0·1239	0·512484±5	−3·0	**1·1**		48	226	0·615	0·710102±7	1·0		0·704	0·65	9·3
	T135G a	charnockite	4·26	25·06	0·1028	0·512382±19	−5·0	**1·1**		12·1	767	**0·046**	0·704064±8	not appl.	1·0	0·704	0·65	−1·3
4	**T135G b**	charnockite	4·29	25·41	0·1022	0·512380±4	−5·0	**1·1**										
5	**T139G**	meta-qtz-diorite	2·05	9·70	0·1279	0·512511±11	−2·5	**1·1**		0·1	750	**0·000**	0·703222±7	neg.	1·0	0·703	0·65	−7·3
7	**A108G a**	metapelite	6·26	31·22	0·1213	0·512475±10	−3·2	**1·1**		37	211	0·507	0·710588±8	1·3		0·706	0·65	30
	A108G b	metapelite	4·88	21·52	0·1370	0·512610±11	−0·5	**1·1**										
8	**A114-1**	metapelite	6·65	29·95	0·1342	0·512488±14	−2·9	**1·3**		72·15	208	1·003	0·716654±7	1·1		0·707	0·65	51
Umba Steppe																		
9	**A125G**	granitoid gneiss	6·06	27·24	0·1345	0·512362±6	−5·4	**1·5**		15	263	**0·165**	0·705849±10	2·2	1·2	0·704	0·65	8·3
10	**A144-1**	Grt–Bt gneiss	6·83	34·91	0·1184	0·512434±6	−4·0	**1·2**		58	203	0·827	0·712057±7	0·90		0·704	0·65	9·3
	Wami River																	
11	**T144-2**	enderbite	5·67	28·91	0·1185	0·512305±10	−6·5	**1·4**		43	817	**0·152**	0·705157±8	2·1	1·1	0·704	0·65	0·2
Uluguru Mts																		
12	**P1 a**	metapelite	6·15	32·68	0·1137	0·511576±9	−20·7	**2·4**										
	P1 b	metapelite	8·62	48·59	0·1072	0·511557±10	−21·1	**2·3**		36	172	0·607	0·726775±7	3·0		0·721	0·65	247
13	**P9-2**	metapelite	8·53	40·33	0·1279	0·512496±15	−2·8	**1·2**		80	91	2·549	0·729795±9	0·78		0·706	0·65	34
18	**T9**	meta-leucogabbro	1·51	6·19	0·1472	0·512246±12	−7·6	**2·1**		3·12	706	**0·013**	0·705096±8	neg.	1·3	0·705	0·65	17·7
19	**P20-1**	enderbite	7·20	24·82	**0·1754**	0·512783±11	2·8	**1·5**	1·0	0·83	456	**0·005**	0·703277±8	neg.	1·0	0·703	0·65	−7·2
20	**T46G a**	meta-qtz-diorite	2·57	14·03	0·1106	0·511493±5	−22·3	**2·4**		18	683	**0·076**	0·704915±9	neg.	1·2	0·704	0·65	6·7
	T46G b	meta-qtz-diorite	2·49	13·06	0·1151	0·511498±5	−22·2	**2·5**										
21	**P94G**	enderbite	5·72	23·61	0·1465	0·512009±11	−12·3	**2·6**		1·42	323	**0·013**	0·707797±6	neg.	1·8	0·708	0·65	56

Table 1: continued

Fig. 1 no.	Sample no.	Rock type	Sm (ppm)	Nd (ppm)	$^{147}Sm/^{144}Nd$	$^{143}Nd/^{144}Nd$	$\varepsilon_{Nd}\ T_0$	$T_{DM}G^1$ (Ga)	Corr. $T_{DM}G^1$	Rb (ppm)	Sr (ppm)	$^{87}Rb/^{86}Sr$	$^{87}Sr/^{86}Sr$	*T*Sr DM² (Ga)	Corr. *T*Sr DM	Sr initial	at T (Ga)	ε_{Sr} initial
Usagaran belt																		
23	**T65-2**	yoderite schist	1·10	7·42	0·0899	0·510913±15	−33·7	**2·7**		4	4	2·905	0·748838±13	1·1		0·665	2·0	−526
24	**A158-9**	kyanite schist	3·63	18·17	0·1208	0·511338±13	−25·4	**3·0**		138	7	59·108	1·078531±44	0·45		−0·624	2·0	−18890
25	**T69G Mp**	metapelite	7·92	39·14	0·1223	0·511297±10	−26·2	**3·1**		107	161	1·933	0·760968±8	2·2		0·705	2·0	45·15
26	**T69G Mb**	eclogite	2·91	9·53	**0·1849**	0·512534±10	−2·0	**3·3**	2·3	0·46	43	**0·031**	0·702662±7	neg.	2·2	0·702	2·0	−4·9
27	**T70G**	metapelite	7·41	40·03	0·1119	0·511175±5	−28·5	**2·9**		105	157	1·945	0·763085±8	2·2		0·707	2·0	70
29	**A167-16**	metapelite	9·19	34·35	0·**1617**	0·511482±15	−22·6	**4·8**	3·6	43	125	0·998	0·737284±7	2·6		0·709	2·0	91
Lowland migmatites and granulites																		
30	**P6-3**	charnockite	2·35	15·54	0·0912	0·510880±9	−34·3	**2·8**		103	384	0·778	0·731776±8	2·8		0·704	2·5	31
31	**A154G**	charnockite	5·16	31·36	0·0995	0·510934±6	−33·2	**2·9**		16	696	**0·066**	0·704671±8	8·6	2·9	0·702	2·5	10·8
32	**A156-5**	charnockite	4·77	26·86	0·1072	0·511024±8	−31·5	**3·0**		41	270	0·440	0·715468±8	2·4		0·700	2·5	−28
Craton																		
33	**T71-1**	charnockite	2·10	10·31	0·1229	0·511313±10	−25·9	**3·1**		92	386	0·691	0·726995±7	2·7		0·702	2·5	7·4
34	**A159-1 a**	tonalitic gneiss	5·22	28·27	0·1116	0·511153±15	−29·0	**3·0**		120	496	0·701	0·727279±8	2·7		0·702	2·5	3·2
	A159-1 b	tonalitic gneiss	5·31	28·47	0·1127	0·511181±9	−28·4	**3·0**										
35	**A164-1**	granodiorite	3·97	22·46	0·1068	0·511018±10	−31·6	**3·0**		14	592	**0·068**	0·714823±7	32	4·7	0·712	2·5	154
36	**A183-1**	tonalitic gneiss	2·84	18·34	0·0935	0·510770±11	−36·4	**3·0**		20	822	**0·070**	0·705213±8	8·7	2·9	0·703	2·5	16·5

Errors are 2σ. Samples with parent/daughter ratios in bold typeface have been used in calculations, but do not yield reliable model ages.

¹Model age calculated after Goldstein *et al.* (1984). Calculation of Nd model ages in this study uses the following algorithm after Goldstein *et al.* (1984): $T_{DM} = 1/\lambda \ln (1 + \{[0{\cdot}51316 - (^{143}Nd/^{144}Nd)_{meas.}]/[0{\cdot}214 - (^{147}Sm/^{144}Nd)_{meas.}]\})$, where $\lambda = 6{\cdot}54 \times 10^{-12}\,yr^{-1}$ (DePaolo, 1988), 0·51316 is modern-day $^{143}Nd/^{144}Nd$ value of depleted mantle, 0·214 is $^{147}Sm/^{144}Nd$ of DM in the model of Goldstein *et al.* (1984). Calculation of corrected Nd model ages uses the following algorithm [after Milisenda *et al.* (1988, 1994)]: $T_{DM} = 1/\lambda \ln [1 + (\{0{\cdot}51316 - (^{143}Nd/^{144}Nd)_{meas.} - [\exp(\lambda x T_{corr}) - 1](^{147}Sm/^{144}Nd)_{meas.} - 0{\cdot}12\})/(0{\cdot}214 - 0{\cdot}12)]$, where T_{corr} is time of metamorphism and change of parent/daughter ratio (used for corrected model ages and Sr initial calculation; value given in the second last column), 0·12 is average $^{147}Sm/^{144}Nd$ ratio of the continental crust (Taylor & McLennan, 1985). Samples with sample numbers in bold typeface are used in diagrams.

²Model age calculated after the same algorithm as used for Nd model ages for extraction from the depleted upper mantle which evolved linearly with a Rb/Sr atomic ratio of 0·027 ($^{87}Rb/^{86}Sr$ isotopic ratio of 0·0459) to a modern value of $^{87}Sr/^{86}Sr = 0{\cdot}702$ (Faure, 1986) from BABI, the 'primordial' initial value of $^{87}Sr/^{86}Sr$ isotopic composition for the Earth (0·69898) at 4·6 Ga. Corrected Sr model ages are corrected for change of Rb/Sr ratio during a geological event with an average crustal $^{87}Rb/^{86}Sr$ ratio of 0·4098 of the continental crust (Faure, 1986), following the same algorithm as corrected Nd model ages above. They appear in an extra column.

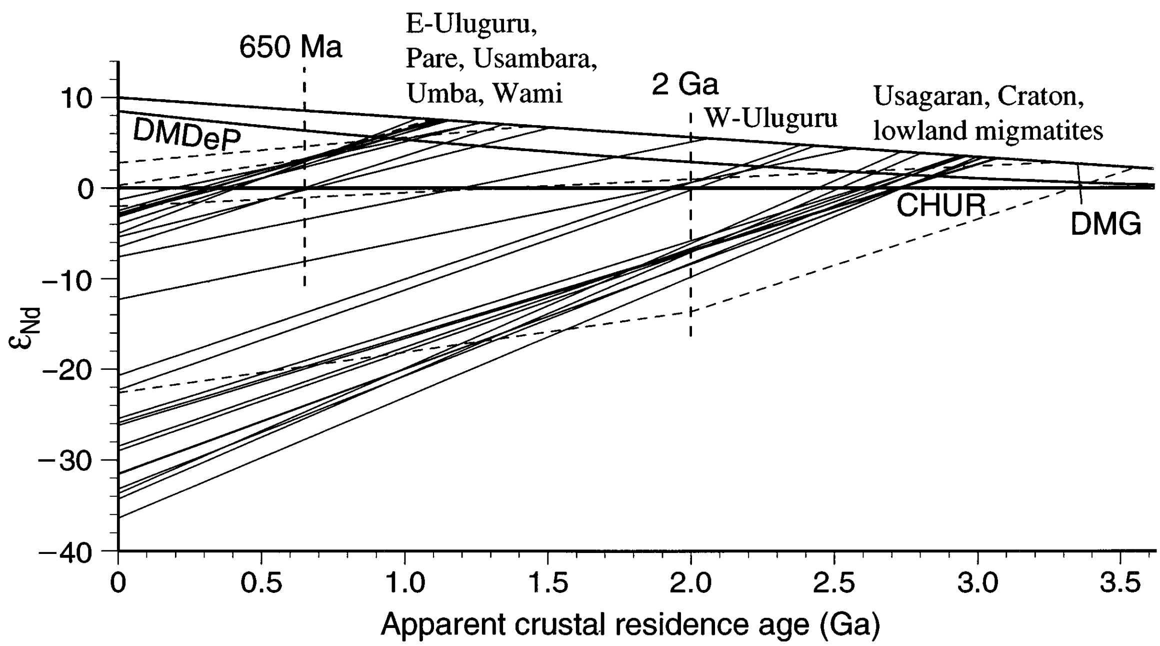

Fig. 2. Nd evolution diagram for Tanzanian high-grade gneisses with ε_{Nd} plotted vs time. Isotopic evolution for samples with $^{147}Sm/^{144}Nd$ ratios higher than 0·15 is plotted as broken lines. The isotope evolution lines for depleted mantle models are calculated for the models proposed by DePaolo (1981) and Goldstein *et al.* (1984).

the models of Goldstein *et al.* (1984) and DePaolo (1981) is about 200 Ma (see Fig. 2).

$^{147}Sm/^{144}Nd$ ratios of most of the Tanzanian samples (Table 1, Fig. 3) are in the typical range for crustal rocks of 0·09–0·13 (Taylor & McLennan, 1985) and similar to those found by Milisenda *et al.* (1988, 1994) in the Pan-African granulites of Sri Lanka, which have a mean $^{147}Sm/^{144}Nd$ value of 0·12. For samples with $^{147}Sm/^{144}Nd$ ratios >0·15, as observed in one eclogite sample (T69G Mb), one enderbite (P20-1) and two garnet-rich metapelites (A167-16 and A16G), corrected Nd model ages were also calculated assuming a pre-metamorphic average crustal $^{147}Sm/^{144}Nd$ of 0·12 following the procedure outlined by Milisenda *et al.* (1994). However, because of the possibility that these high Sm/Nd values are caused by alteration in the crust and because of the higher uncertainty related to low-angle intersection with the depleted mantle evolution curve, these samples are not taken into account in the discussion of crustal residence ages.

There is little correlation between sample provenance and the parent/daughter ratio except for lower $^{147}Sm/^{144}Nd$ values that are restricted to meta-granitoids of the craton and migmatites and granulites of the lowlands.

Evolution models for distinct geochemical Sr reservoirs are harder to define, because of the much larger variability in isotope composition and concentration of Sr. A recent review of available isotope data by Hofmann (1997) supports $^{87}Sr/^{86}Sr$ of 0·720 for average continental crust and 0·702 for a present-day depleted mantle endmember. This $^{87}Sr/^{86}Sr$ value for the depleted mantle is supported by mantle endmember calculations of Allègre *et al.* (1983). These isotopic ratios have been used to calculate the parent/daughter ratios for linear evolution of depleted mantle and continental crust from a bulk Earth value at 4·6 Ga. Sr model ages for the Tanzanian samples were then calculated (Table 1) from intersection with the depleted mantle evolution. For samples with low parent/daughter ratios (<0·2) which do not yield meaningful model ages, a correction procedure similar to that used for Nd has been applied for comparison, using the Rb/Sr value of average continental crust.

The Tanzanian high-grade rocks show an enormous variation in $^{87}Rb/^{86}Sr$ (Fig. 3). Many orthogneisses and charnockites have $^{87}Rb/^{86}Sr$ values which are similar to the depleted mantle value, making model age calculations impossible. Except for mafic gneisses with high $^{147}Sm/^{144}Nd$, which may have retained their mantle signature, this is interpreted as an indication for depletion of Rb, possibly during crustal processes (e.g. high-grade metamorphism), especially where low parent/daughter ratio is coupled with very radiogenic Sr. Trace element ratios also show that Rb has been depleted with respect to K and Sr in many of the orthogneiss samples of this study

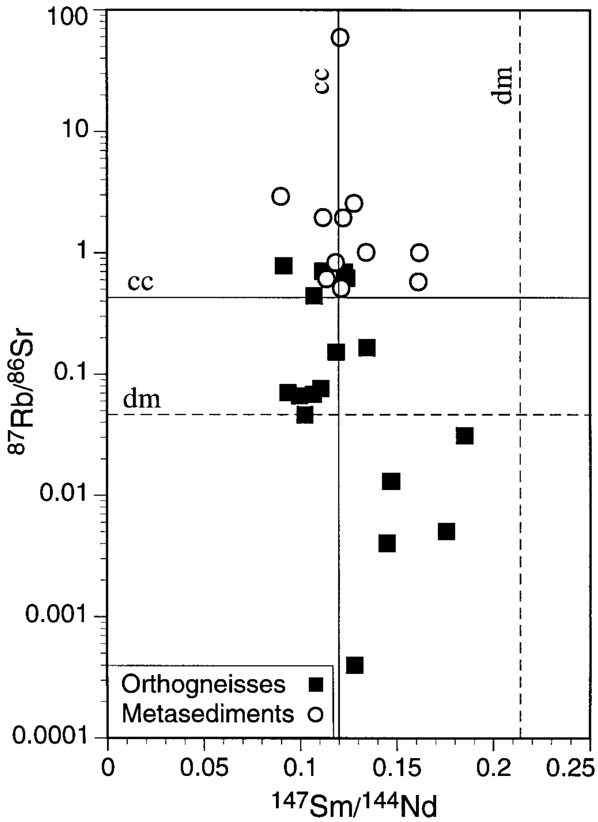

Fig. 3. $^{147}Sm/^{144}Nd$ plotted vs $^{87}Rb/^{86}Sr$ (note log-scale) for high-grade rocks from Tanzania. Shown for comparison are the parent/daughter ratios for average continental crust (cc) and depleted mantle (dm). For Sm–Nd, cc value is taken from Taylor & McLennan (1985), dm value from Goldstein *et al.* (1984). Ratios for Rb–Sr are calculated from modern $^{87}Sr/^{86}Sr$ of 0·720 for cc and 0·702 for dm (Hofmann, 1997). The samples show little variability in Sm/Nd, but a large spread in Rb/Sr, with many Rb/Sr ratios of orthogneisses well below the depleted mantle value.

(Appel, 1996), possibly during high-grade metamorphism. The high-grade metasediments on the other hand display $^{87}Rb/^{86}Sr$ values which are consistent with average continental crust or higher; none show signs of depletion or values envisaged for the lower continental crust.

Nd isotopes

The regional distribution of Nd model ages is portrayed on a simplified geological map of eastern Tanzania (Fig. 4) showing the most important geological units of eastern Tanzania and some of the granulite complexes in the Mozambique Belt. This distribution of apparent crustal residence ages suggests that there are at least three age provinces within the orogenic belt, each with its own pre-metamorphic history.

The first group has model ages between 2·7 and 3·3 Ga and is represented by meta-granitoids of the craton together with eclogite- and amphibolite-facies rocks from the Usagaran domain. No distinction of crustal history is possible between the samples from the Archean craton and the granulite-facies orthogneisses from the lowlands of the Mozambique Belt. This patchy distribution of Archean Nd model ages suggests that Archean crustal material played an important role in the constitution of the belt and that it was not everywhere mixed with younger crustal material. Remelting and mixing with juvenile melts are hence not likely to have been pervasive processes.

Four metasedimentary samples from the Usagaran belt have Nd model ages that are indistinguishable from that of the Archean craton and thus these rocks are probably derived from this source without the addition of major amounts of new crust. An outlier to this well-defined group is the garnet-rich metapelite sample from the Great Ruaha River (sample A167-16) with a $^{147}Sm/^{144}Nd$ ratio of 0·16, which yields a model age higher than the age of the Earth. More than one fractionation event has affected this sample as it may have undergone more than one cycle of weathering, sedimentation and metamorphism. It is therefore excluded from further discussion.

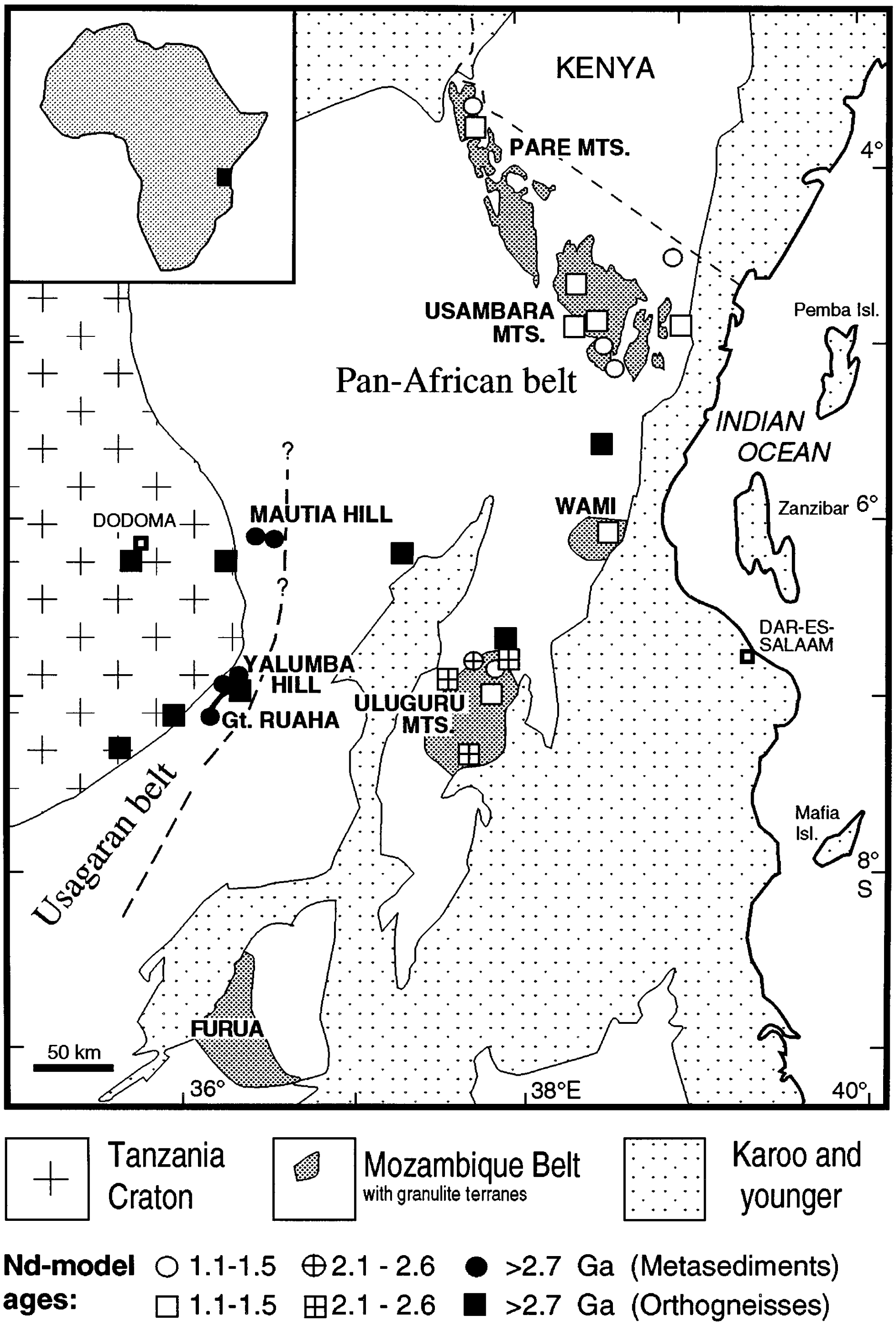

Fig. 4. Simplified geological map of eastern Tanzania, showing the distribution of Nd model ages calculated after Goldstein *et al.* (1984). It should be noted that Archean Nd model ages cover not only the granitoids of the Tanzania Craton and the metapelites and eclogite of the Usagaran Belt, but also amphibolite-facies migmatites and some granulites of the lowlands in the Pan-African belt. Rocks with young model ages <1·5 Ga occur only in the granulites of NE Tanzania and the eastern Uluguru Mts, whereas all samples from the western Uluguru Mts yield significantly older model ages.

The second group of Nd model ages clusters between 1·1 and 1·5 Ga and is restricted to the granulite areas of NE Tanzania (Pare, Usambara, Umba, Wami) and the granulites of the eastern Uluguru Mts. This group of granulites can be explained as juvenile additions to the crust between 1·5 and 1·1 Ga, or alternatively as a product of mixing of juvenile material during the Pan-African orogenic cycle (~0·65 Ga; Möller *et al.*, 1994) with small amounts of pre-existing crustal material possibly from the Archean Tanzania craton and the Usagaran Belt, or other older terranes today separated from Tanzania by the Indian Ocean. Other explanations without mixing of older components include the derivation from a mantle with curvilinear evolution (DePaolo, 1981) as shown in Fig. 2, where the isotope evolution lines of most granulites cross the depleted mantle curve of DePaolo (1981) between 0·9 and 1·0 Ga. Another possibility is extraction early in the Pan-African orogenic cycle from a less depleted mantle, which may be expected where subcontinental lithosphere is involved. This was invoked as the source of 740 Ma granulites in Sudan, which are interpreted as the northern extension of the Mozambique Belt (Stern & Dawoud, 1991).

The third group of samples indicates mixing between crustal material of different ages. Regionally restricted to the northwestern and southern part of the Uluguru Mts, these samples show Nd model ages between 2·1 and 2·6 Ga. This may indicate a localized crust formation event during this time, but as these model ages are restricted to a narrow band between the Proterozoic rocks of the eastern Uluguru Mts and older Archean rocks of the surrounding lowlands it is possible that they result from mixing of cratonic and/or Usagaran material with some Proterozoic juvenile material during the Pan-African orogeny. This interpretation will be further investigated with the help of whole-rock Sr isotope systematics and the Pb isotope composition of feldspar from this area.

It is striking that a possible boundary between two of these crustal domains lies within the Uluguru Mts granulite complex. This tentative boundary is not clearly defined in the Pan-African metamorphic history (Appel *et al.*, 1998), but appears to be masked, notwithstanding that there is an apparent lithological contrast between the eastern and western Uluguru Mts (Sampson & Wright, 1964). The eastern Uluguru Mts consist of a supracrustal sequence with dominant marbles and metapelites, whereas the western part of the granulite complex is dominated by orthogneisses and a large anorthosite intrusion, and metasediments are scarce. This lithological boundary may coincide with the age province boundary. A similar situation has been found in the granulites of Sri Lanka, where Pan-African metamorphic gradients cross lithologic and age province boundaries outlined by Nd isotope mapping (Raase & Schenk, 1994).

Sr isotopes

Calculation of initial $^{87}Sr/^{86}Sr$ ratios for high-grade polymetamorphic rocks is complicated by the possible changes in the Rb/Sr ratios during crustal processes discussed above. Therefore only the time-integrated effects are displayed in a conventional isochron diagram (Fig. 5). A rigorous interpretation of the data arrangement in terms of geologically meaningful ages is not advisable because the large area covered in this study and the variety of rock types certainly preclude cogenetic origin or homogenization events affecting all samples. Nevertheless, it can be noted that the data align along two major trends with different slopes and slight differences in the initial ratios (Fig. 5). However, both trends are almost entirely based on the few metapelite samples with high Rb/Sr ratios. One of these trends has a low initial $^{87}Sr/^{86}Sr$ ratio of about ~0·704 and follows a reference line corresponding to an age of ~740 Ma. Although it cannot be assumed that this subset (consisting of the granulites from the Pare and Usambara Mts, the Umba Steppe, Wami River and the eastern Uluguru Mts) rigorously fulfills the criteria for geological significance of whole-rock isochrons, it can be observed that all samples with Nd model ages <1·6 Ga plot close to this Pan-African reference line. The alignment could suggest partial isotopic homogenization during the Pan-African high-grade metamorphism (pervasive fluids released by metamorphic dehydration reactions), or a juvenile common mantle source for these samples. The latter seems unlikely because metasediments also fall on this reference line, and would then have had little time to be eroded and deposited, then buried and metamorphosed together with the orthogneisses. Another reason for the metasediments to fall on an errorchron may be equilibration with seawater Sr during deposition.

The second array has a higher initial $^{87}Sr/^{86}Sr$ ratio of 0·705 and follows a reference line corresponding to an age of ~2100 Ma which may be the result of incomplete Sr isotopic equilibration during the Usagaran–Ubendian orogeny at 2 Ga. Except for the samples from Mautia Hill (T65-2 and A158-9), the granodiorite from the border of the Archean craton (A164-1) and the mafic eclogite (sample T69G Mb), all samples with Nd model ages >2 Ga define this errorchron. On an expanded scale (Fig. 5b), the samples with the low Rb/Sr ratios show that the initial value of the 2·1 Ga errorchron is poorly defined. Samples with low $^{87}Sr/^{86}Sr$ ratios have low parent/daughter ratios that may have been acquired during earlier (pre-2 Ga) high-grade metamorphic events. The very high Rb/Sr ratio of kyanite schist A158-9 and the unusually low Sr content of both metasediments from Mautia Hill (Table 1, Fig. 3) suggest that both samples lost Sr, possibly during sedimentation or later metamorphism. This is consistent with the observation that both samples

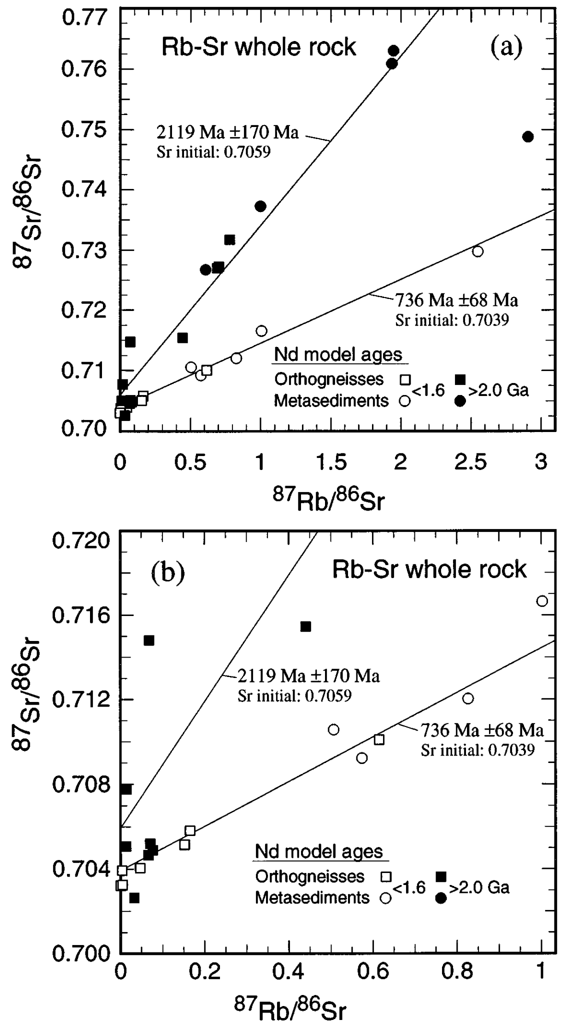

Fig. 5. Rb–Sr isochron diagrams. Errors are calculated with the Isoplot program of Ludwig (1994). (a) Samples with Nd model ages <1·6 Ga plot on an errorchron of ~740 Ma with an initial $^{87}Sr/^{86}Sr$ ratio of 0·704. Most samples with Nd model ages >2 Ga plot on an errorchron of ~2100 Ma with an initial $^{87}Sr/^{86}Sr$ ratio of 0·706. (See text for discussion.) (b) Enlargement for samples with low isotope ratios.

plot below the 2·1 Ga reference line (A158-9 out of range of Fig. 5) defined by the other samples with high Nd model ages, and yield Sr model ages well below their Nd model age (Table 1, Fig. 6). Eclogite sample T69G Mb has very low Rb/Sr as well as Sr isotopic composition ($^{87}Sr/^{86}Sr$ initial = 0·702) suggesting that this metabasaltic rock was derived from a source with mantle-like Sr isotopic composition and not contaminated by crustal material. A granodiorite from the border of the Archean craton (A164-1) exhibits high Sr isotopic composition ($^{87}Sr/^{86}Sr$ = 0·715) despite its low Rb/Sr ratio, thus plotting far above the 2·1 Ga reference line. This deviation may be attributed either to derivation from an evolved crustal source or alternatively to Rb depletion by an event late enough to leave time for the development of the high $^{87}Sr/^{86}Sr$ ratio, such as a Pan-African metamorphic overprint.

Given the relative mobility of Rb and Sr and the uncertainties in Sr mantle evolution because of isotope inhomogeneities in the mantle, good correlations of Sr with Pb or Nd isotopic signature cannot be expected. Only Sr model ages which fall in the range of Nd model ages calculated for the respective crustal province and are not younger than the metamorphic age that is known to have affected the sample are considered to be meaningful here.

A good correlation of Nd with Sr model ages is observed for samples from Mozambique Belt granulites with Nd model ages <2 Ga. These samples fall on the younger (740 Ma) Sr-errorchron and have normal crustal or

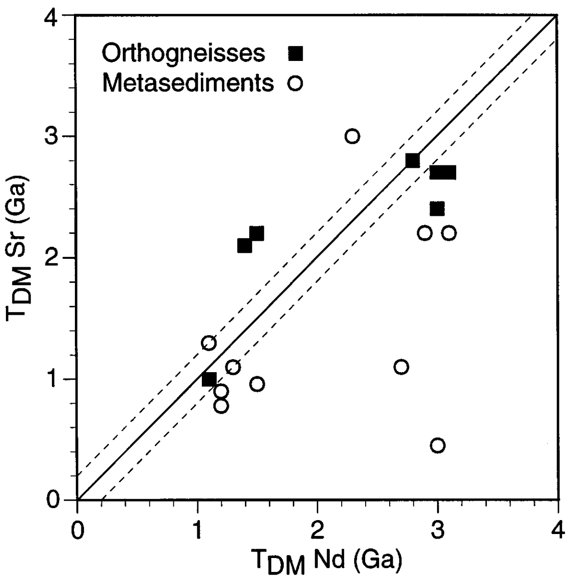

Fig. 6. Comparison of Nd model ages and Sr model ages. Samples which did not yield meaningful model ages (negative or >4·5 Ga) are not shown (11 samples for Sr, one sample for Nd). Sr model ages deviate strongly from Nd model ages. Reference line is drawn for matching results, with stippled lines indicating deviation of ±200 Ma.

higher Rb/Sr ratios, which also yield Sr model ages <2 Ga (Table 1, Fig. 6). However, most of these rocks are metasediments. This result confirms the interpretation based on Nd isotopes that these granulite-facies rocks have Mid to Late Proterozoic formation ages and contain no or very little contribution from pre-existing material with a prolonged crustal history.

Assuming that Rb depletion caused the very low Rb contents in some samples, model ages can be calculated assuming the original Rb/Sr ratio and knowing the time of Rb depletion (see Table 1). Some 'corrected' Sr model ages from Pare and Usambara Mts granulites which are estimated in this way actually do show good correlation with Nd model ages (Table 1), suggesting that Rb depletion indeed occurred during that metamorphic event (see discussion above). Most of the craton samples, the migmatitic granulites from the Mozambique Belt lowlands and some of the Usagaran samples show apparent Sr crustal residence ages consistently older than their respective age of metamorphism (Fig. 6) and agree within 500 Ma with Nd model ages. However, most other Sr model ages do not yield satisfactory results; some differ widely from the Nd model ages and are also not consistent with the Pb isotope composition of leached feldspars. It is thus apparent that Sr model ages are difficult to interpret if calculated without knowledge of other isotopic data and can only yield supplementary age information.

Pb systematics of feldspars

Table 2 lists the Pb isotope data obtained on feldspars in this study. The Pb isotope ratios from leached feldspar separates allow distinction of four groups of basement rocks in eastern Tanzania. The first group is defined by granitoids of the craton together with eclogite- and amphibolite-facies rocks from the Usagaran domain. The feldspars from this group have strongly retarded common Pb (Fig. 7), which is consistent with the Archean Nd model ages between 2·7 and 3·6 Ga. Samples from the craton as well as the Usagaran Belt lie above the Stacey & Kramers (1975) (S&K) Pb-evolution curve, and require extraction from an S&K source at or before 3 Ga. The primitive character of the Pb in the feldspars indicates that the feldspars are still pristine and thus the cratonic rocks did not undergo metamorphism in post-Archean time. The samples from the Usagaran domain can be interpreted to be derived from this Archean material and these feldspars equilibrated with the whole rocks during the Ubendian–Usagaran orogeny at ~2 Ga (Möller *et al.*, 1995) as indicated by their elevated $^{206}Pb/^{204}Pb$ ratios and the slope of the data array connecting the feldspars from the Usagaran domain with the craton samples in Fig. 7a. This interpretation is consistent with the data array in the $^{208}Pb/^{204}Pb$ vs $^{206}Pb/^{204}Pb$ diagram (Fig. 7b), where the data points follow the S&K evolution curve. The Nd model ages are also consistent with this interpretation of the Usagaran domain as mainly reworked Archean material. One sample from the border of the Archean craton with the Usagaran Belt (A164-1, labeled Craton border in Fig. 7) plots slightly below the S&K reference curve and to more radiogenic values compared with the rest of the craton samples. This position may be explained by later re-equilibration of this sample

Table 2: Feldspar Pb isotope data

Fig. 1 no.	Sample no.	Rock type	Mineral	$^{206}Pb/^{204}Pb$	$^{207}Pb/^{204}Pb$	$^{208}Pb/^{204}Pb$	Pb model age (Ga)*	μ value
Pare Mts								
1	A16G	metapelite	Kfs	17·362 ± 7	15·452 ± 7	37·074 ± 19	0·67	9·32
2	A26-2	calcsilicate	Pl	17·962 ± 2	15·555 ± 2	37·686 ± 5	0·41	9·60
Usambara Mts								
3	T121G	charnockite	Kfs	17·994 ± 2	15·555 ± 2	37·460 ± 5	0·39	9·59
4	T135G	charnockite	Pl	17·539 ± 3	15·466 ± 2	37·105 ± 6	0·56	9·32
5	T139G	meta-qtz-diorite	Pl	17·677 ± 4	15·483 ± 3	37·240 ± 8	0·48	9·35
6	T137-1	metapelite	Kfs	17·385 ± 4	15·508 ± 3	37·310 ± 1	0·76	9·58
7	A108G	metapelite	Kfs	17·359 ± 2	15·479 ± 1	37·147 ± 4	0·72	9·45
8	A114-1	metapelite	Kfs	17·244 ± 1	15·461 ± 1	37·100 ± 2	0·78	9·41
Umba Steppe								
9	A125G	granitoid gneiss	Kfs	18·153 ± 3	15·583 ± 3	38·128 ± 8	0·32	9·67
10	A144-1	Grt–Bt gneiss	Kfs	17·970 ± 2	15·520 ± 2	38·113 ± 5	0·33	9·43
Wami River								
11	T144-2	enderbite	Pl	17·051 ± 2	15·425 ± 2	36·664 ± 5	0·86	9·32
Uluguru Mts								
12	P1	metapelite	Kfs	17·746 ± 5	15·713 ± 5	37·413 ± 1	0·86	10·42
13	P9-2	metapelite	Kfs	18·175 ± 1	15·562 ± 1	37·301 ± 2	0·26	9·57
14	T28-1	metapelite	Kfs	16·496 ± 1	15·281 ± 1	36·308 ± 3	1·03	8·87
15	T25-1	marble	Kfs	16·781 ± 4	15·399 ± 4	36·481 ± 11	1·02	9·33
16	P8-7	calcsilicate	Pl	17·594 ± 1	15·646 ± 1	37·297 ± 2	0·85	10·16
17	P88-5	calcsilicate	Pl	17·330 ± 1	15·497 ± 1	36·818 ± 3	0·78	9·55
18	T9	metaleucogabbro	Pl	17·439 ± 17	15·637 ± 15	37·269 ± 35	0·95	10·19
	T9 b	metaleucogabbro	Pl	17·291 ± 7	15·590 ± 6	37·239 ± 14	0·98	10·03
19	P20-1	enderbite	Pl	17·811 ± 4	15·514 ± 3	37·173 ± 8	0·44	9·45
20	T46G	meta-qtz-diorite	Pl	15·652 ± 6	15·293 ± 6	35·770 ± 15	1·75	9·69
21	P94G	enderbite	Pl	17·282 ± 3	15·583 ± 3	37·199 ± 7	0·97	10·00
Usagaran belt								
22	T73-3	enderbite	Pl	16·209 ± 4	15·560 ± 5	35·640 ± 12	1·70	10·77
27	T70G	metapelite	Kfs	15·947 ± 13	15·579 ± 12	35·530 ± 28	1·94	11·30
28	A167-9	metabasite	Pl	16·040 ± 9	15·436 ± 9	35·392 ± 20	1·66	10·15
29	A167-16	metapelite	Kfs	16·539 ± 7	15·664 ± 7	35·851 ± 16	1·63	11·05
Lowland migmatites and granulites								
30	P6-3	charnockite	Kfs	14·806 ± 3	14·972 ± 4	35·914 ± 9	1·95	8·67
31	A154G	charnockite	Kfs	14·402 ± 2	15·107 ± 3	40·927 ± 7	2·56	11·25
32	A156-5	charnockite	Pl	14·262 ± 4	14·949 ± 5	36·094 ± 1	2·45	9·93
Craton								
33	T71-1	charnockite	Kfs	14·123 ± 1	15·058 ± 1	33·763 ± 4	2·75	12·25
34	A159-1	tonalitic gneiss	Kfs	14·084 ± 1	15·002 ± 1	33·845 ± 3	2·71	11·61
35	A164-1	granodiorite	Kfs	15·294 ± 1	15·144 ± 1	35·436 ± 4	1·80	9·15
36	A183-1	tonalitic gneiss	Kfs	13·946 ± 3	14·932 ± 4	34·068 ± 9	2·75	11·45

Error is the absolute $2\sigma_{mean}$ within-run precision on the last digit of the measured value. Bold type indicates the analysis used in diagrams from duplicate samples. Pl, plagioclase; Kfs, K-feldspar.
*Pb model ages and μ value calculated with Isoplot program (Ludwig, 1994).

during the Ubendian or Pan-African orogeny, an interpretation that is consistent with its Sr isotope systematics.

The second group of samples is well constrained by Pb isotope composition and has Nd model ages between 1·1 and 1·5 Ga (Pare, Usambara, Umba, Wami and the eastern Uluguru Mts granulites). The Pb data from these samples plot in a tight array below the S&K evolution curve and to the right of the 1·0 Ga geochron in the ^{207}Pb/^{204}Pb vs ^{206}Pb/^{204}Pb diagram (Fig. 7a). These granulites plot along a secondary isochron, calculated for μ = 9·7, with isotopic evolution between 1·3 and 0·5 Ga, consistent with a whole-rock Pb evolution for the timespan between the average Nd model age and the post-metamorphic closure of feldspar for Pb. The data are similar to, but span a wider field than, Pb isotopic data from juvenile Pan-African rocks (dated by U–Pb on zircon at 570–660 Ma) from the Arabian–Nubian shield (Stacey *et al.*, 1980; Stacey & Stoeser, 1983).

The spread in ^{207}Pb/^{204}Pb ratio exhibited by the youngest group of samples is still extremely narrow and only half the spread of modern mid-ocean ridge basalt (MORB) (Hofmann, 1997). This tight array precludes incorporation of older crustal components because those would have produced a much larger spread in the ^{207}Pb/^{204}Pb ratios, as is found in the samples from the western Uluguru Mts (see below). Like the Archean samples, these young samples also follow the S&K evolution curve in the ^{208}Pb/^{204}Pb vs ^{206}Pb/^{204}Pb diagram (Fig. 7b). Samples from the eastern Uluguru Mts (Fig. 1, 13–19), some of which have low Nd as well as low Sr crustal residence ages, plot in the same region of the diagram as the NE Tanzania granulites of the second Pb isotope group. They also fall on the same secondary isochron (Fig. 7a), which is interpreted as further evidence for a common crustal history of these domains and a boundary between different crustal age domains within the Uluguru Mts.

The third group (western part of the Uluguru Mts) shows a large variation in the ^{207}Pb/^{204}Pb ratios, indicating the influence of old reworked crust. The steep array in the ^{207}Pb/^{204}Pb vs ^{206}Pb/^{204}Pb diagram requires the influence of material similar to that exposed in the Usagaran domain or the Archean craton. As indicated by the tight array in the ^{208}Pb/^{204}Pb vs ^{206}Pb/^{204}Pb diagram (Fig. 7b), Archean crustal material of the type of the lowland migmatites and granulites did not contribute significantly to the protoliths of these rocks. The combination of the Pb isotopes with the intermediate Nd model ages and the large spread in the Nd model ages indicates that these rocks from the Uluguru Mts formed as a result of mixing of crustal material of different residence ages.

The fourth group are the lowland migmatites and granulites in the Mozambique Belt with Archean Nd model ages indistinguishable from those of the craton and similar Rb–Sr whole-rock characteristics. These three migmatitic granulites show elevated ^{208}Pb/^{204}Pb ratios but plot close to the samples from the craton in the ^{207}Pb/^{204}Pb vs ^{206}Pb/^{204}Pb diagram. The high ^{208}Pb/^{204}Pb ratios require at least a two-stage Pb evolution, the first stage of which would be similar to the samples from the craton. The second stage requires an almost complete loss of U, but not Th, from the whole rock in the Archean as the most likely cause of their primitive uranogenic Pb isotope ratios. As indicated by geochronologic data on metamorphic minerals (Möller, 1995), the migmatites were later metamorphosed during the Pan-African orogeny. The high κ values of the whole rocks then led to high ^{208}Pb/^{204}Pb ratios and to little change of ^{206}Pb/^{204}Pb ratios in the feldspars compared with samples from the Archean craton in the timespan between the early U depletion event and the Pan-African metamorphic event. This implies that depleted Archean crustal material was incorporated and reworked in the Mozambique Belt during Pan-African times and that the lowland migmatites and granulites already experienced an early first metamorphic event, probably in the Archean.

Earlier studies of Pb isotopes on galenas and feldspars from rocks of the Archean Tanzania Craton and from the Early Proterozoic Ubendian Belt to the west of the craton (Robertson, 1973) complement the data presented here. Taking some uncertainties from different analytical techniques and lower analytical precision of the older data into account, the galena data are consistent with the data on leached feldspars from this study and support the notion that the Pan-African metamorphic event had a strong influence on the Early Proterozoic provinces of the Ubendian as well as the Usagaran domains.

The Pb isotopic compositions of galena (Fig. 8) from the Nyanzian volcanics of the Archean Tanzania Craton (Robertson, 1973) are similar to the three most primitive Pb isotopic compositions obtained from the granitoid gneisses of the craton presented above (Fig. 7) and are consistent with a growth curve with μ = 11. Most of the isotopic ratios of galena are more primitive than the feldspar data, which may reflect their insensitivity to later equilibration. They plot at a possible convergence point of the Archean feldspar data and may represent a common Pb source at 2·8 Ga. This consistency indicates that the Archean Pb isotope composition may be characteristic for a larger portion of the granitic gneisses that can be grouped with the Archean Karagwe–Ankolean system of the traditional Tanzanian stratigraphy (Harpum, 1970) and can today be found as far east as sample A154 in the Mozambique Belt (location 31 in Fig. 1).

Galena from mineralized veins in the central Ubendian (Fig. 8a) yields relatively young Pb model ages in a tight range of 1·5–1·7 Ga with μ values equal to or slightly higher than the evolution curve suggested by Stacey &

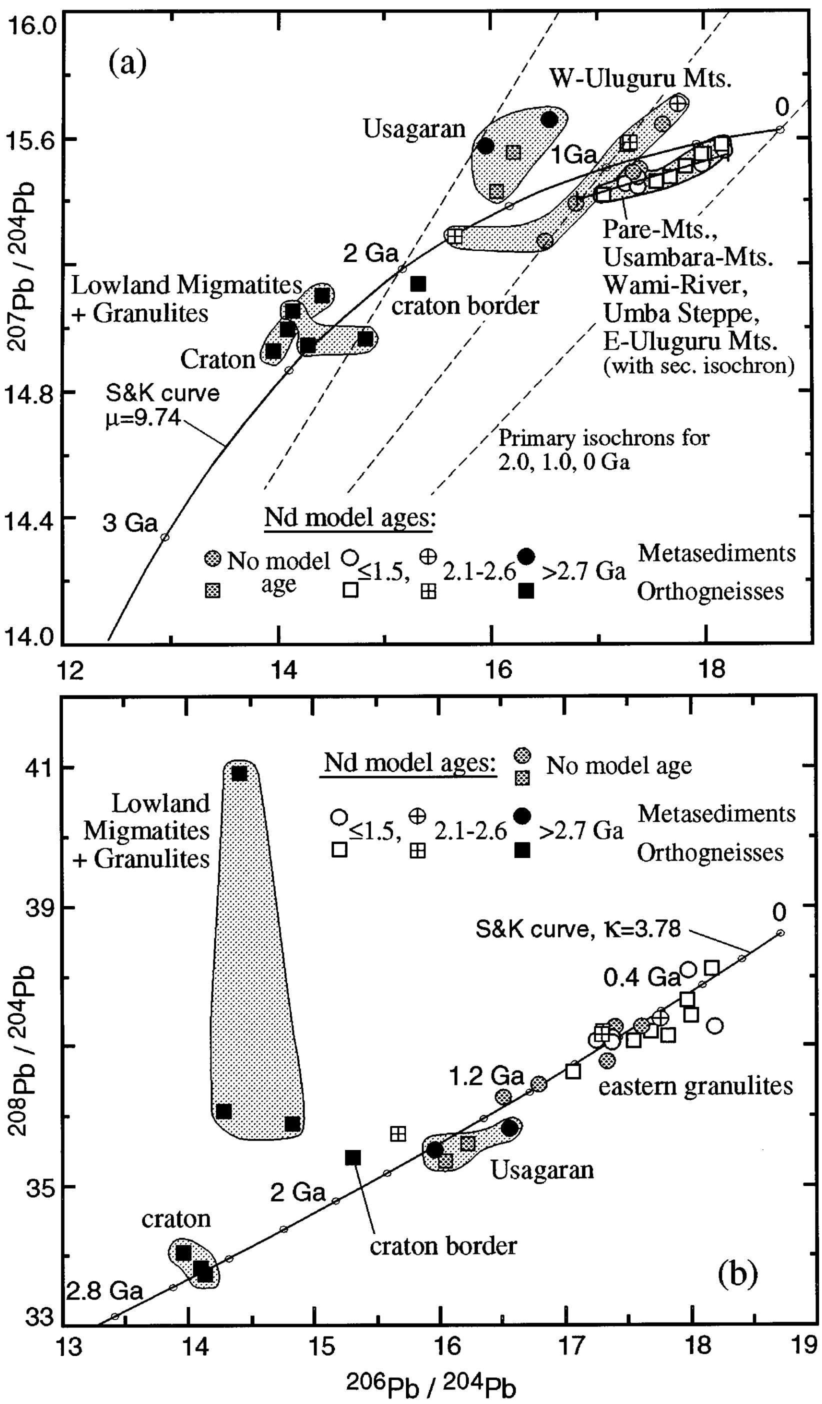

Fig. 7. (a) $^{207}Pb/^{204}Pb$ vs $^{206}Pb/^{204}Pb$ diagram for leached feldspar from high-grade gneisses in Tanzania with the Pb isotope growth curve of Stacey & Kramers (1975) and primary isochrons for reference. Calculated with the Isoplot software of Ludwig (1994). (b) $^{208}Pb/^{204}Pb$ vs $^{206}Pb/^{204}Pb$ diagram for leached feldspar from high-grade gneisses from Tanzania with the Pb isotope growth curve of Stacey & Kramers (1975) for reference. Data points are combined into groups to stress isotopic characteristics and trends.

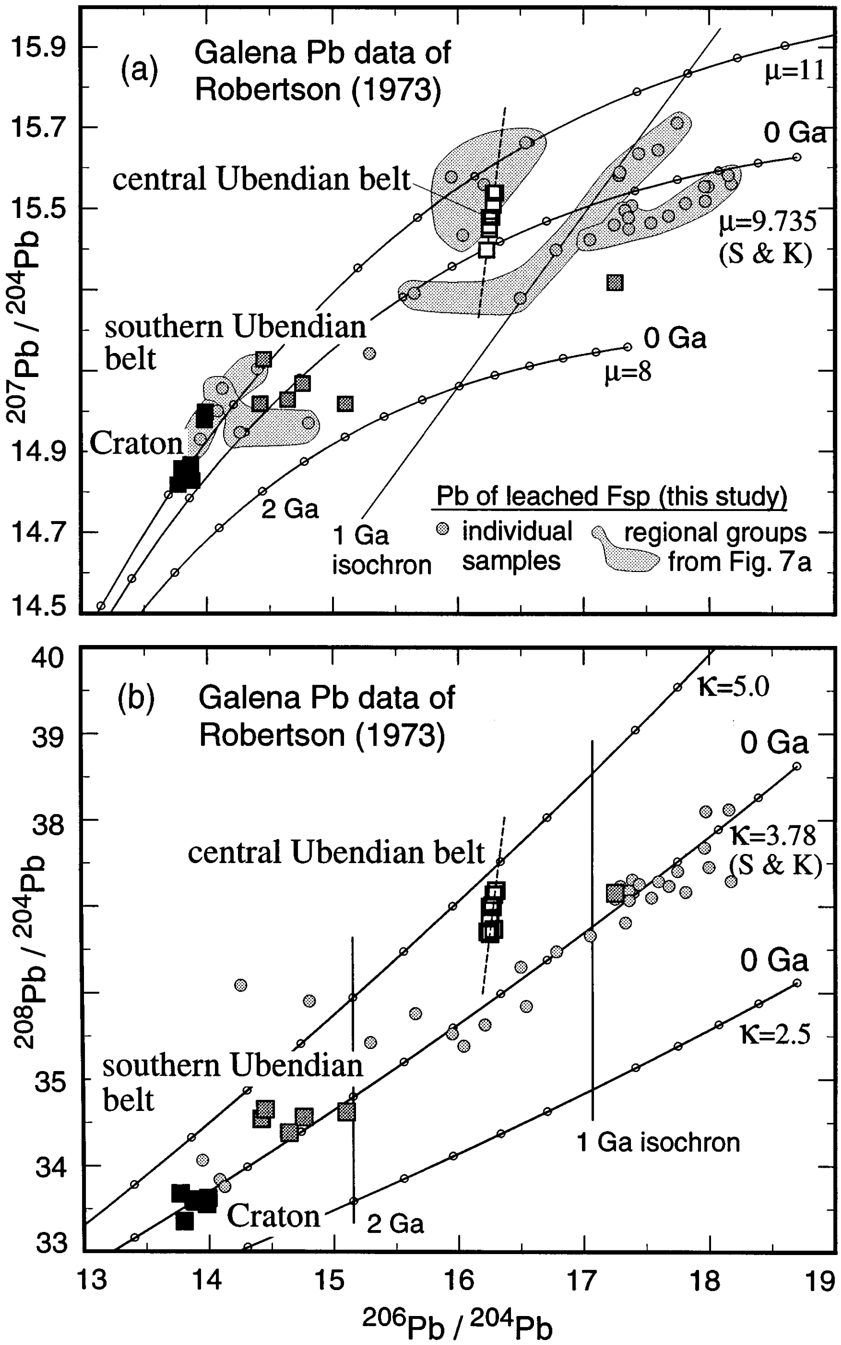

Fig. 8. (a) $^{207}Pb/^{204}Pb$ vs $^{206}Pb/^{204}Pb$ diagram for galena data of Robertson (1973) for rocks from the Tanzania Craton and the Ubendian Belt (squares), with the Pb isotope growth curve of Stacey & Kramers (1975), growth curves for μ values of 11 and 8·0 and primary isochrons for reference. (b) $^{208}Pb/^{204}Pb$ vs $^{206}Pb/^{204}Pb$ diagram for galena data of Robertson (1973) for rocks from the Tanzania Craton and the Ubendian Belt, with the Pb isotope growth curve of Stacey & Kramers (1975), growth curves for κ values of 5 and 2·5, and the 1·0 Ga primary isochron for reference. Pb isotope data for leached feldspar of this study (circles) are shown for comparison in both diagrams.

Kramers (1975). This is consistent with the data obtained on the leached feldspars from the Usagaran, which also lie above the S&K curve and yield only slightly different Pb model ages (Figs 7a and 8a).

The galena Pb isotope data from the southern Ubendian Belt (the Lupa goldfield on the southwestern fringe of the Tanzania Craton) show considerable scatter in the $^{207}Pb/^{204}Pb$ vs $^{206}Pb/^{204}Pb$ diagram (Fig. 8a). One sample obviously formed during Pan-African time. It shows high $^{206}Pb/^{204}Pb$ that can be explained by Pb evolution between 2·0 and 0·65 Ga, at a μ value slightly lower than the S&K curve (~9). The $^{207}Pb/^{204}Pb$ vs $^{206}Pb/^{204}Pb$ distribution of the other southern Ubendian samples may be explained by evolution during the time from the metamorphic event in the craton (at 2·5 Ga) and the 2·0 Ga event in the Ubendian–Usagaran along growth curves with widely different μ values. In the $^{208}Pb/^{204}Pb$ vs $^{206}Pb/^{204}Pb$ diagram (Fig. 8b), the samples can be interpreted in the same manner as in $^{207}Pb/^{204}Pb$ vs $^{206}Pb/^{204}Pb$ space. Samples from the Nyanzwa (craton) and the southern Ubendian Belt (Lupa–Mbeya) lie very close to the model Pb evolution curve of Stacey & Kramers (1975), whereas the samples from the areas in the central and northern Ubendian Belt (Mpanda and Karema) show higher $^{208}Pb/^{204}Pb$ ratios (at κ value of ~4), with a steep positive trend which is probably due to fractionation during analysis.

DISCUSSION

Combination of Nd model ages with Pb isotopic composition of leached feldspars reveals distinct and previously unrecognized crustal tracts in the Mozambique Belt of Tanzania. Archean crustal material is not restricted to the Tanzania Craton itself but prevails in the Usagaran–Ubendian Belt and is also widespread in the eastern part of the Mozambique Belt, which has been affected by granulite-facies metamorphism during the Pan-African orogeny (Coolen *et al.*, 1982; Möller *et al.*, 1994). In this latter area there is a significant amount of juvenile material formed during a relatively short time-span in the Middle to Late Proterozoic. However, despite the widespread occurrence of these juvenile granulite complexes, they do not form the majority of outcrop in the Mozambique Belt. The emplacement in their present-day relation with the adjoining Archean gneisses may in fact be due to nappe piling late in the Pan-African orogeny during final collision of East and West Gondwana.

Mixing of Proterozoic and Archean crust occurred only locally along a narrow band which is now partly exposed in the western Uluguru Mts. The isotope data thus provide strong evidence for most Proterozoic crustal growth in eastern Tanzania by lateral accretion of ~1·0–1·3 Ga old material onto an Archean nucleus. This accretion must have been completed before the Pan-African orogeny, as no structural or metamorphic discontinuity can be correlated with the age domain boundary within the Uluguru Mts. There is no known field evidence for this geodynamic interpretation, probably because any such evidence was destroyed by the intense deformation and metamorphism during the Pan-African orogeny.

The combination of different isotope systems in the same samples is clearly extremely useful for investigations into the crustal history of high-grade metamorphic terranes. A good example for this is the Uluguru Mts granulites, where a single granulite terrane may be subdivided in terms of crustal residence time, whereas there is no structural or petrological evidence for such a distinction. Long crustal residence times for granulites and amphibolite-facies migmatites between the Pan-African granulite mountains suggest a complex regional distribution of crustal age domains within the Mozambique Belt. It is essential to recognize this complexity when reconstructing the plate-tectonic history of the Pan-African belt.

Crustal age domains in central Gondwana

A combination of the data presented here with previously published Nd results can be used to reconstruct parts of the tectonic and crustal growth history of Gondwana in an attempt to derive similar geodynamic interpretations as for Tanzania for a wider region and identify targets for further combined isotope studies. The relevant regions that once constituted part of central Gondwana occur around today's Indian Ocean (East Africa, India, Antarctica, and possibly SW Australia).

Published Nd whole-rock data from East Africa are scarce. Only 15 results are available for Kenya, Uganda and Madagascar, none are available for Mozambique and Malawi. Recent studies on granulites, gneisses and granites from the craton, the Usagaran Belt and the Pan-African belt of Tanzania by Maboko (1995), and Maboko & Nakamura (1996) encompass 32 samples and provide an important addition to the database presented here. Their results on the Tanzania Craton and lowland migmatites and granulites are fully consistent with this study in their small range of Archean ages between 2·8 and 3·1 Ga. Variably deformed granitoids from the Usagaran Belt exhibit slightly younger Nd model ages than samples from the craton, explained by mixing of juvenile, mantle-derived melts with pre-existing Archean crust during the Usagaran orogeny (Maboko & Nakamura, 1996). The Usagaran metasediments of this study yield older Nd model ages (2·7–3·1 Ga, indistinguishable from results of the Archean Craton) than these Usagaran granitoids (2·4–3·0 Ga) studied by Maboko & Nakamura (1996), which indicates that little or no juvenile material of the Usagaran orogeny was eroded to contribute to the metasediments. The Mid-Proterozoic Nd model ages found in the W Uluguru Mts by Maboko (1995) can also be explained by mixing of different source rocks, as evident from the Nd, Sr and Pb isotopic results of this study for the same region. However, contrary to the interpretation of Maboko (1995), we argue that the Mid-Proterozoic Nd model ages in the Mozambique Belt may not by themselves be regarded as the result of a mixed source history. Mid-Proterozoic upper intercepts of U–Pb zircon data on granulite-facies orthogneisses from the Wami River granulite complex (Maboko *et al.*, 1985) render their explanation as juvenile additions to the crust at that time equally possible. It has clearly been shown by Nd model age and Pb isotope data of this study that the W Uluguru Mts cannot serve as a model for all Pan-African granulite complexes in Tanzania because they are isotopically distinct from the granulites of NE Tanzania as well as the E Uluguru Mts. The Pb isotopic signature of leached feldspars from the lowland migmatites and granulites distinguishes these from the other samples with Archean Nd model ages, those of the Usagaran Belt and the craton. This difference suggests that the pre-Pan-African crustal history of the Archean components in the MB is different from the history of the Tanzanian craton and cannot be regarded as simply the result of Pan-African reworking. Loss of U in all three lowland migmatite samples studied here did probably occur during an Archean high-grade event.

For correlations on a larger scale, ~380 whole-rock Nd results were compiled (Table B1, Appendix B) from the available literature on Precambrian rocks of other fragments of central Gondwana (East Africa, Madagascar, South India, Sri Lanka, Antarctica). The compiled data are summarized in a series of histograms (Fig. 9). All Nd model ages were recalculated using the depleted mantle model of Goldstein *et al.* (1984) and Nd isotopic ratios renormalized to a $^{146}Nd/^{144}Nd$ ratio of 0·7219 where necessary. Samples with $^{147}Sm/^{144}Nd > 0{\cdot}15$ are not plotted or discussed because of potential alteration in the crust (see discussion above).

The compiled Nd data for high-grade rocks are presented in a simplified map of central Gondwana (Fig. 10), modified after Kriegsman *et al.* (1993) and Windley *et al.* (1994). Four types of crustal domains can be distinguished on the basis of the Nd model ages in this part of Gondwana.

(1) Strictly Archean domains with Nd model ages >2·6 Ga (e.g. Tanzania and Karnataka craton, Tanzania lowland migmatites, Napier complex, Madras, Nilgiri and northern block of South India, Western Nile complex of Uganda), some of which show very narrow age ranges of no more than 400 my (Madras and Nilgiri Block, Tanzania Craton and lowland migmatites) or a near-normal distribution (Napier complex). The Napier complex is the oldest of these, with a protracted Archean igneous and metamorphic history. Narrow age bands distinguish cratonic areas which have not been affected by later magmatism or tectonism. The bimodal age distribution of the Karnataka craton and the 'transition zone' is only visible after rejection of samples with high Sm/Nd. Yet this distribution may still reflect crustal components with different mantle extraction age and mixing and could aid identification of an age domain boundary within this Archean age domain.

(2) Domains with a wide range of Nd model age ranges from Middle Proterozoic to Early Archean (Trivandrum and Madurai Block, Palghat–Cauvery shear zone, the Highland Complex of Sri Lanka, Androyan granulites of SE Madagascar, Usagaran Belt of Tanzania). The Nd model ages are dominantly Archean, but some are as low as 1·4 Ga (Trivandrum Block in South India) and suggest that these regions have been subject to several crust formation events which produced a wide range of apparent crustal residence ages. These areas include polymetamorphic areas, and could mark the proximal part of active continental margins on old Archean nuclei (Usagaran Belt).

(3) Crustal domains which have Nd model ages from the Late Proterozoic to the Early Proterozoic or Late Archean (1·0–2·6 Ga) suggesting extensive mixing of material with different crustal residence ages (Rayner complex, Heimefrontfjella, Sverdrupfjella, Vijayan and Wanni complex, western Kenya, W Uluguru Mts), but little involvement of Archean crust. These may be distal parts of Proterozoic orogenic belts girdling Archean cratons or domains which include Proterozoic accreted terranes not spatially resolved.

(4) Strictly Mid to Late Proterozoic areas (1·0–1·7 Ga) with no Nd model ages older than 1·7 Ga (Pare and Usambara Mts, Umba Steppe, E Uluguru Mts, the basement of central Kenya, Sør–Rondane Mts, and the granitoids of the Lützow–Holm complex). These may constitute Proterozoic arcs or the distal zone of late Proterozoic continental margins with limited mixing.

It has to be noted, however, that this classification, based on Nd model ages alone, is not sensitive enough to distinguish differences in age distribution between the Rayner complex and the Heimefrontfjella (Table 3) in Antarctica and the Wanni and Vijayan complex in Sri Lanka (Fig. 9g) which all fall into the category (3), although these have distinct age spectra. The Heimefrontfjella and Vijayan complex are the younger (more juvenile?) terranes.

It is also important to note that metasediments and metaigneous rocks of some domains can exhibit distinct age characteristics, e.g. in the Lützow–Holm Bay and in the Usagaran Belt, where metasediments are older than the metaigneous rocks of these domains. This trend suggests that the metasediments were derived from an older exposed hinterland and that some, but not necessarily all, igneous material is a juvenile addition to the crust.

We propose that the narrow zone of mixing of crustal units with different ages extends from the W Uluguru Mts of Tanzania to the Sekerr area of W Kenya. In Kenya, the mixing zone is close to the craton and no equivalent to the Tanzanian Usagaran belt seems to be

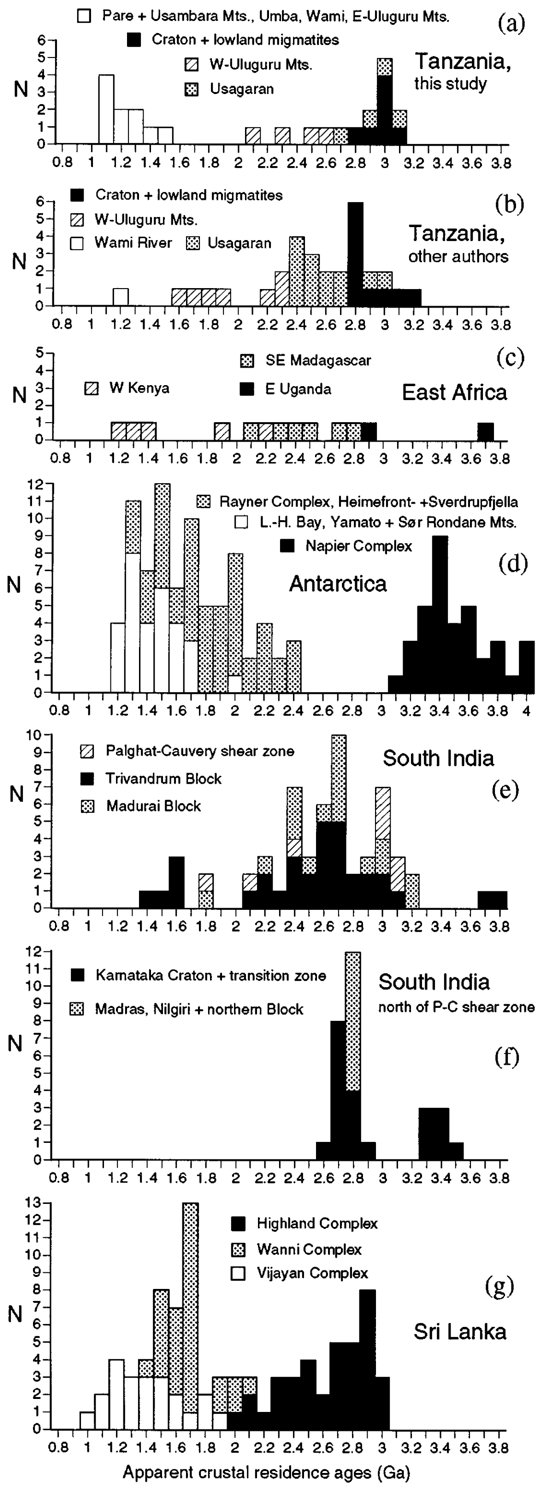

Fig. 9. Histograms of Nd model ages for: (a) Tanzania (29 from this study, Table 1); (b) Tanzania, other workers (Ben Othman *et al.*, 1984; Maboko, 1995; Maboko & Nakamura, 1996); (c) East Africa with Madagascar (Ben Othman *et al.*, 1984; Harris *et al.*, 1984; Paquette *et al.*, 1994); (d) Antarctica with the Napier complex in Enderby Land (DePaolo *et al.*, 1982; McCulloch & Black, 1984; Black *et al.*, 1986; Black & McCulloch, 1987), the Rayner complex (Black *et al.*, 1987), the Lützow–Holm complex (Tanaka *et al.*, 1985; Owada *et al.*, 1994; Shiraishi *et al.*, 1995), the Yamato Mts (Zhao *et al.*, 1995), the Sør–Rondane Mts (Shiraishi & Kagami, 1992), and the Heimefrontfjella (Arndt *et al.*, 1991) and Sverdrupfjella (Moyes *et al.*, 1993) from western Dronning Maud Land; (e and f) South India (Drury *et al.*, 1983; Bernard-Griffiths *et al.*, 1987; Peucat *et al.*, 1989, 1993; Choudhary *et al.*, 1992; Santosh *et al.*, 1992; Harris *et al.*, 1994; Brandon & Meen, 1995; Jayananda *et al.*, 1995; Unnikrishnan-Warrier *et al.*, 1995; Bhaskar Rao *et al.*, 1996); (g) Sri Lanka (Milisenda *et al.*, 1988, 1994; Burton & O'Nions, 1990; Kagami *et al.*, 1990). All data recalculated to modern-day $^{143}Nd/^{144}Nd$ ratio of 0·512638 for CHUR where necessary. Nd model ages calculated with the depleted mantle model of Goldstein *et al.* (1984).

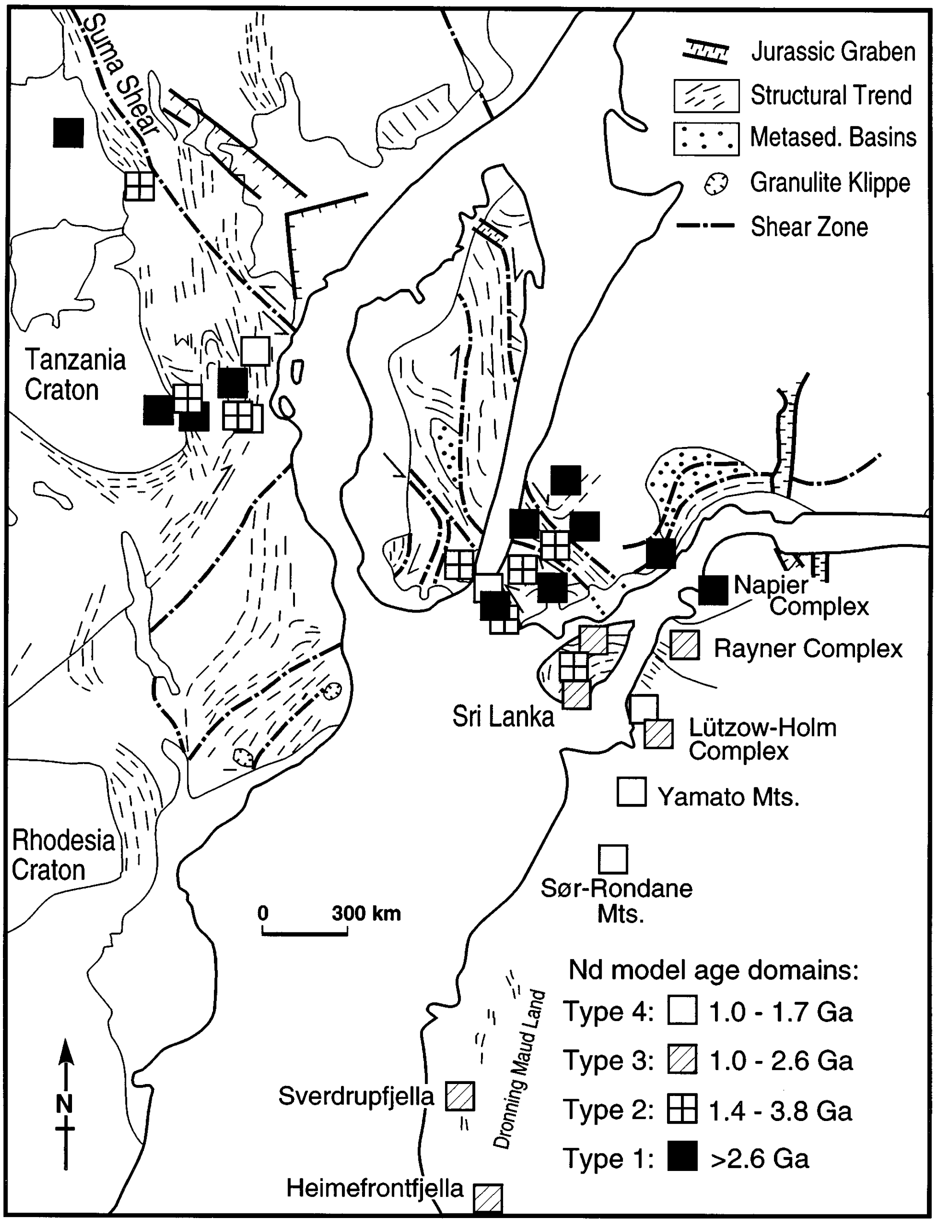

Fig. 10. Simplified map of part of central Gondwana with Nd model age provinces for Precambrian basement rocks. The reconstruction is based on Lawver & Scotese (1987). Map modified after Kriegsman (1993) and Windley *et al.* (1994).

present. However, further south the lack of Nd data from South Tanzania and Mozambique and the restriction of Nd data for Madagascar to the SE corner of this important Gondwana fragment preclude further correlations of early continental crust in these directions.

The continuation of the Proterozoic Sri Lankan geological units into the Rayner and Lützow–Holm complexes of Antarctica (Kriegsman, 1993; Shiraishi *et al.*, 1994) is reflected in the similarity of crust formation ages in the Lützow–Holm complex and Sør Rondane Mts with the Vijayan complex (despite the trend to higher Nd model ages in the latter) and between the Rayner complex areas with the Wanni Complex. The Karnataka craton, the Madras and Nilgiri blocks, all exhibiting strictly Archean Nd model ages and Archean granulite-facies metamorphism, can be proposed to be equivalents of the Napier complex in the sense that for these areas crustal growth ended in the Archean. The crust-formation history of SE Madagascar could be similar to that of the Archean Highland Complex of Sri Lanka, but the large spread in Nd model ages for the Trivandrum Block, which has also experienced Pan-African high-grade metamorphism and lies between Madagascar and Sri Lanka in the Gondwana reconstruction, does not allow a more detailed discussion. The Nd model age map (Fig. 10) together with the compiled Nd model age histograms (Fig. 9) may be used to look for areas that have not been studied extensively yet and may be rewarding targets. An example is the Trivandrum Block, which appears to have segments of very different crustal residence age and possibly a complex age distribution similar to the Mozambique Belt of Tanzania.

GENERAL CONCLUSIONS

The Nd data on the Tanzanian Mozambique Belt of this study allow the distinction of crustal provinces that had not been identified previously. Whereas other isotopic systems on minerals (U–Pb, K–Ar) may yield information on the latest metamorphic event and subsequent cooling, the apparently limited fractionation of Sm and Nd during crustal processes makes Nd model ages useful guides to the pre-metamorphic history of high-grade terranes. The extensive database on Pan-African granulites from Sri Lanka (Milisenda *et al.*, 1988, 1994) combined with the results presented in this study provide strong support that the Sm/Nd ratios in crustal rocks do not change significantly during granulite-facies metamorphism. This conclusion is in contrast to the suggestions of Burton & O'Nions (1990) and Choudhary *et al.* (1992) from the study of *in situ* charnockites where evidence was found for a change in the Sm/Nd ratio during the granulite-facies imprint. The average Sm/Nd ratio of all studied Sri Lankan and Tanzanian granulites is indistinguishable from the average Sm/Nd ratio of sediments (Taylor & McLennan, 1985; McLennan & Hemming, 1992). Thus, it is not necessary or even useful in the interpretation of Nd isotope data to correct all results on granulites to a pre-metamorphic Sm/Nd atomic ratio of 0·19 (^{147}Sm/^{144}Nd ratio of 0·11) as advocated by Harris *et al.* (1994), unless field relations and textures such as *in situ* charnockitization suggest that we should do so.

Whole-rock Sr data can also provide protolith information rather than give the age of metamorphism, but their usefulness is hampered by large variations in the parent/daughter ratios, which can be the result of different crustal processes. The results obtained on the Tanzanian samples show some linear errorchron alignment of the data similar to the results of Milisenda *et al.* (1994) for Sri Lanka, but no exact age significance can be attached to these correlations. However, some Sr model ages or alternatively the initial isotopic ratios calculated for the time of Pan-African metamorphism can serve as an additional indicator of the presence or absence of a pre-Pan-African crustal history of the samples from the Mozambique Belt. In this respect, the Sr data support the subdivision of the Mozambique Belt made on the basis of Nd isotopic data.

The Pb isotopic composition of leached feldspars preserves a time-integrated memory of the U–Th–Pb history of the sample before the last homogenization event, in this case the last metamorphic overprint. The Pb data can thus provide important additional information which supplements the Nd and Sr whole-rock isotope data. The more complex U–Th–Pb isotopic system allows the distinction of subgroups within the groups distinguished by Nd isotopes. Pb data may yield crucial evidence for (DeWolf & Mezger, 1994) or against (Pare and Usambara Mts, this study) mixed-source Nd isotopic composition, an uncertainty that otherwise troubles the interpretation of Nd model ages as crust-forming events (Arndt & Goldstein, 1987). Hence, Pb isotope data are an invaluable tool for the refinement of discussions on the recognition of crustal provinces in high-grade gneiss belts.

The data presented here allow a division of the Mozambique Belt into distinct provinces with different geologic and geochemical evolution as outlined in the Discussion. The combination of different isotope systems serves as a particularly powerful tool for the reconstruction of the geochemical evolution of these distinct domains. Extension of this approach to larger parts of Gondwana will allow a more robust reconstruction of ancient terrane boundaries and will lead to a reliable model for the evolution and the geodynamic setting of Precambrian crustal domains.

ACKNOWLEDGEMENTS

This paper represents part of the doctoral dissertation of A. M. and is a contribution to IGCP 348. We sincerely thank P. Appel for making geochemical data available, for discussions, and for his collaboration during the long months of fieldwork. Research permits from the Tanzanian Commission for Science and Technology and support of the University of Dar-es-Salaam (Dr S. Muhongo) and the Geological Survey of Tanzania are gratefully acknowledged. We thank L. D. Ashwal, J. D. Kramers and R. J. Stern for their thorough reviews, which helped improve the original manuscript. A. M. thanks B. Mocek for help with the final draft. Research was financially supported by the Deutsche Forschungsgemeinschaft (DFG) through Grants Sche 265-2/5 and Sche 265-6/1.

REFERENCES

Allègre, C. J., Hart, S. R. & Minster, J.-F. (1983). Chemical structure and evolution of mantle and continents determined by inversion of

Nd and Sr isotopic data, II. Numerical experiments and discussion. *Earth and Planetary Science Letters* **66,** 191–213.

Appel, P. (1996). Hochdruckgranulite und Eklogite im Mozambique Belt von Tansania: eine petrologische und geochemische Studie. Ph.D. Thesis, Christian-Albrechts-Universität Kiel, Germany.

Appel, P., Möller, A. & Schenk, V. (1998). High-pressure granulite-facies metamorphism in the Pan-African belt of eastern Tanzania: evidence against tectonic crustal thickening during prograde metamorphism. *Journal of Metamorphic Geology*, in press.

Arndt, N. T. & Goldstein, S. L. (1987). Use and abuse of crust-formation ages. *Geology* **15,** 893–895.

Arndt, N. T., Todt, W., Chauvel, C., Tapfer, M. & Weber, K. (1991). U–Pb zircon age and Nd isotopic composition of granitoids, charnockites and supracrustal rocks from Heimefrontfjella, Antarctica. *Geologische Rundschau* **80,** 759–777.

Bagnall, P. S. (1963). The geology of the North Pare mountains. *Records of the Geological Survey of Tanganyika* **10,** 7–16.

Bagnall, P. S., Dundas, D. L. & Hartley, E. W. (1963). The geology of the Mnazi and Lushoto areas: quarter degree sheets 90 and 109, and part of 73 E. *Records of the Geological Survey of Tanganyika* **11,** 15–17.

Bell, K. & Dodson, M. H. (1981). The geochronology of the Tanzanian shield. *Journal of Geology* **89,** 109–128.

Ben Othman, D., Polvé, M. & Allègre, C. J. (1984). Nd–Sr isotopic composition of granulites and constraints on the evolution of the lower continental crust. *Nature* **307,** 510–515.

Bernard-Griffiths, J., Jahn, B.-M. & Sen, S. K. (1987). Sm–Nd isotopes and REE geochemistry of Madras granulites, India: an introductory statement. *Precambrian Research* **37,** 343–355.

Bhaskar Rao, Y. J. B., Chetty, T. R. K., Janardhan, A. S. & Gopalan, K. (1996). Sm–Nd and Rb–Sr ages and P–T history of the Archean Sittampundi and Bhavani layered meta-anorthosite complexes in Cauvery shear zone, south India: evidence for Neoproterozoic reworking of Archean crust. *Contributions to Mineralogy and Petrology* **125,** 237–250.

Black, L. P. & McCulloch, M. T. (1987). Evidence for isotopic equilibration of Sm–Nd whole-rock systems in early Archaean crust of Enderby Land, Antarctica. *Earth and Planetary Science Letters* **82,** 15–24.

Black, L. P., Sheraton, J. W. & James, P. R. (1986). Late Archaean granites of the Napier Complex, Enderby Land, Antarctica: a comparison of Rb–Sr, Sm–Nd and U–Pb isotopic systematics in a complex terrain. *Precambrian Research* **32,** 343–368.

Black, L. P., Harley, S. L., Sun, S. S. & McCulloch, M. T. (1987). The Rayner Complex of East Antarctica: complex isotopic systematics within a Proterozoic mobile belt. *Journal of Metamorphic Geology* **5,** 1–26.

Brandon, A. D. & Meen, J. K. (1995). Nd isotopic evidence for the position of southernmost Indian terranes within East Gondwana. *Precambrian Research* **70,** 269–280.

Burke, K., Dewey, J. F. & Kidd, W. S. F. (1977). World distribution of sutures—the sites of former oceans. *Tectonophysics* **40,** 69–99.

Burton, K. & O'Nions, R. K. (1990). The timescale and mechanism of granulite formation at Kurunegala, Sri Lanka. *Contributions to Mineralogy and Petrology* **106,** 66–89.

Cameron, A. E., Smith, D. H. & Walker, R. L. (1969). Mass spectrometry of nanogram-size samples of lead. *Nature* **41,** 525–526.

Choudhary, A. K., Harris, N. B. W., Van Calsteren, P. W. C. & Hawkesworth, C. J. (1992). Pan-African charnockite formation in Kerala, South India. *Geological Magazine* **129,** 257–264.

Coolen, J. J. M. M. M. (1980). Chemical petrology of the Furua granulite complex, southern Tanzania. *GUA Papers of Geology* **13,** 258.

Coolen, J. J. M. M. M., Priem, H. N. A., Verdurmen, E. A. T. & Verschure, R. H. (1982). Possible zircon U–Pb evidence for Pan-African granulite-facies metamorphism in the Mozambique Belt of southern Tanzania. *Precambrian Research* **17,** 31–40.

DePaolo, D. J. (1981). Neodymium isotopes in the Colorado Front Range and crust–mantle evolution in the Proterozoic. *Nature* **291,** 193–196.

DePaolo, D. J. (1988). *Neodymium Isotope Geochemistry*. Berlin: Springer.

DePaolo, D. J., Manton, W. I., Grew, E. S. & Halpern, M. (1982). Sm–Nd, Rb–Sr and U–Th–Pb systematics of granulite facies rocks from Fyfe Hills, Enderby Land, Antarctica. *Nature* **298,** 614–618.

DeWolf, C. P. & Mezger, K. (1994). Lead isotope analyses of leached feldspars: constraints on the early crustal history of the Grenville Orogen. *Geochimica et Cosmochimica Acta* **58,** 5537–5550.

Drury, S. A., Holt, R. W., Van Calsteren, P. W. C. & Beckinsale, R. D. (1983). Sm–Nd and Rb–Sr ages for Archean rocks in western Karnataka, South India. *Journal of the Geological Society of India* **24,** 454–459.

Faure, G. (1986). *Principles of Isotope Geology*. New York: John Wiley.

Gabert, G. (1973). Über granitische Gesteine des Dodoman und Usagaran im südlichen Hochland von Tanzania (Ostafrika). *Geologisches Jahrbuch* **B6,** 3–50.

Gabert, G. & Wendt, I. (1974). Datierung von granitischen Gesteinen im Dodoman- und Usagaran-System und in der Ndembera-Serie (Tanzania). *Geologisches Jahrbuch* **B11,** 3–55.

Goldstein, S. L., O'Nions, R. K. & Hamilton, P. J. (1984). A Sm–Nd isotopic study of atmospheric dusts and particulates from major river systems. *Earth and Planetary Science Letters* **70,** 221–236.

Harpum, J. R. (1970). Summary of the geology of Tanzania Part 5: Structure and geotectonics of the Precambrian. *Memoirs of the Geological Survey of Tanganyika* **1**.

Harris, N. B. W., Hawkesworth, C. J. & Ries, A. C. (1984). Crustal evolution in north-east and east Africa from model Nd ages. *Nature* **309,** 773–776.

Harris, N. B. W., Santosh, M. & Taylor, P. N. (1994). Crustal evolution in South India: constraints from Nd isotopes. *Journal of Geology* **102,** 139–150.

Hofmann, A. W. (1997). Mantle geochemistry: the message from oceanic volcanism. *Nature* **385,** 219–228.

Holmes, A. (1951). The sequence of Precambrian orogenic belts in south and central Africa. *Proceedings of the 18th International Geological Congress, Vol. 14*. London: Assoc. Seros. Geol. Afr., pp. 254–269.

Jayananda, M., Janardhan, A. S., Sivausaubrmanian, P. & Peucat, J. J. (1995). Geochronologic and isotopic constraints on granulite formation in the Kodaikanal area, southern India. In: Yoshida, M. & Santosh, M. (eds) *India and Antarctica During the Precambrian. Geological Society of India, Memoir* **34,** 373–390.

Kagami, H., Owada, M., Osanai, Y. & Hiroi, Y. (1990). Preliminary geochronological study of Sri Lankan rocks. In: Hiroi, Y. & Motoyoshi, Y. (eds) *Study of Geologic Correlation Between Sri Lanka and Antarctica: Interim Report Japan–Sri Lanka Joint Research*, pp. 55–70.

Kennedy, W. Q. (1964). The structural differentiation of Africa in the Pan-African (±500 my) tectonic episode. *Annual Report on Scientific Results, University of Leeds* **8**, 48–50.

Key, R. M., Charsley, T. J., Hackman, B. D., Wilkinson, A. F. & Rundle, C. C. (1989). Superimposed Upper Proterozoic collision-controlled orogenies in the Mozambique Orogenic Belt of Kenya. *Precambrian Research* **44,** 197–225.

Kriegsman, L. (1993). Geodynamic evolution of the Pan-African lower crust in Sri Lanka: structural and petrological investigations into a high-grade gneiss terrain. *Geologica Ultraiectina* **114**.

Krogh, T. E. (1973). A low-contamination method for hydrothermal decomposition of zircon and extraction of U and Pb for isotopic age determinations. *Geochimica et Cosmochimica Acta* **37,** 485–494.

Kröner, A. (1977). Precambrian mobile belts of S and E Africa—ancient sutures or sites of ensialic mobility? A case for crustal evolution towards plate tectonics. *Tectonophysics* **40,** 101–135.

Lawver, L. A. & Scotese, C. R. (1987). A revised reconstruction of Gondwanaland. In: McKenzie, G. W. (ed.) *Gondwana Six: Structure, Tectonics and Geophysics*. Washington, DC: American Geophysical Union, pp. 17–23.

Lenoir, J.-L., Liégeois, J. P., Theunissen, K. & Klerckx, J. (1994). The Palaeoproterozoic Ubendian shear belt in Tanzania: geochronology and structure. *Journal of African Earth Sciences* **19,** 169–184.

Liew, T. C. & Hofmann, A. W. (1988). Precambrian crustal components, plutonic associations, plate environment of the Hercynian Fold Belt of central Europe: indications from a Nd and Sr isotopic study. *Contributions to Mineralogy and Petrology* **98,** 129–138.

Ludwig, K. R. (1994). Isoplot—a plotting and regression program for radiogenic-isotope data, Version 2.75. *US Geological Survey Open File Report* **91-445**.

Ludwig, K. R. & Silver, L. T. (1977). Lead-isotope inhomogeneity in Precambrian igneous K-feldspars. *Geochimica et Cosmochimica Acta* **41,** 1457–1471.

Maboko, M. A. H. (1995). Neodymium isotopic constraints on the protolith ages of rocks involved in Pan-African tectonism in the Mozambique Belt of Tanzania. *Journal of the Geological Society, London* **152,** 911–916.

Maboko, M. A. H. & Nakamura, E. (1996). Nd and Sr isotopic mapping of the Archaean–Proterozoic boundary in southeastern Tanzania using granites as probes for crustal growth. *Precambrian Research* **77,** 105–115.

Maboko, M. A. H., Boelrijk, N. A. I. M., Priem, H. N. A. & Verdurmen, E. A. T. (1985). Zircon U–Pb and biotite Rb–Sr dating of the Wami river granulites, eastern granulites, Tanzania: evidence for approximately 715 Ma old granulite-facies metamorphism and final Pan-African cooling approximately 475 Ma ago. *Precambrian Research* **30,** 361–378.

McCulloch, M. T. & Black, L. P. (1984). Sm–Nd isotopic systematics of Enderby Land granulites and evidence for the redistribution of Sm and Nd during metamorphism. *Earth and Planetary Science Letters* **71,** 46–58.

McLennan, S. M. & Hemming, S. (1992). Samarium/neodymium elemental and isotopic systematics in sedimentary rocks. *Geochimica et Cosmochimica Acta* **56,** 887–898.

Meert, J. G. & van der Voo, R. (1996). Paleomagnetic and $^{40}Ar/^{39}Ar$ study of the Sinyai dolerite, Kenya: implications for Gondwana assembly. *Journal of Geology* **104,** 131–142.

Meert, J. G., van der Voo, R. & Ayub, S. (1995). Paleomagnetic investigation of the Neoproterozoic Gagwe lavas and Mbozi complex, Tanzania and the assembly of Gondwana. *Precambrian Research* **74,** 225–244.

Mezger, K., Hanson, G. N. & Bohlen, S. R. (1989). U–Pb systematics of garnet: dating the growth of garnet in the late Archean Pikwitonei granulite domain at Cauchon and Natawahiman lakes, Manitoba, Canada. *Contributions to Mineralogy and Petrology* **101,** 136–148.

Milisenda, C. C., Liew, T. C., Hofmann, A. W. & Kröner, A. (1988). Isotopic mapping of age provinces in Precambrian high-grade terrains: Sri Lanka. *Journal of Geology* **96,** 608–615.

Milisenda, C. C., Liew, T. C. & Hofmann, A. W. (1994). Nd isotopic mapping of the Sri Lanka basement: update, and additional constraints from Sr isotopes. *Precambrian Research* **66,** 95–110.

Miyashiro, A., Aki, K. & Sengör, A. M. C. (1984). *Orogeny*. New York: John Wiley.

Möller, A. (1995). Pan-African granulites and Early Proterozoic eclogites in the Precambrian basement of eastern Tanzania: *P–T–t* history and crustal evolution of the complex Mozambique belt. Ph.D. Thesis, Christian-Albrechts-Universität Kiel, Germany.

Möller, A., Mezger, K. & Schenk, V. (1994). U–Pb dating of metamorphic minerals: age of metamorphism and cooling history of Panafrican granulites and Early Proterozoic eclogites in Tanzania. *European Journal of Mineralogy* **6** (Beiheft 1), 182.

Möller, A., Appel, P., Mezger, K. & Schenk, V. (1995). Evidence for a 2 Ga subduction zone: eclogites in the Usagaran Belt of Tanzania. *Geology* **23,** 1067–1070.

Moyes, A. B., Groenewald, P. B. & Brown, R. W. (1993). Isotopic constraints on the age and origin of the Brattskarvet intrusive suite, Dronning Maud Land, Antarctica. *Chemical Geology* **106,** 453–466.

Muhongo, S. (1991). The Mozambique belt: a polyorogenic mobile belt. *UNESCO Newsletter* **8,** 5–14.

Muhongo, S. M. & Lenoir, J.-L. (1994). Pan-African granulite-facies metamorphism in the Mozambique belt of Tanzania: U–Pb zircon geochronology. *Journal of the Geological Society, London* **151,** 343–347.

Owada, M., Osanai, Y. & Kagami, H. (1994). Isotopic equilibration age of Sm–Nd whole-rock system in the Napier complex (Tonagh Island), East Antarctica. *Proceedings of the NIPR Symposium, Vol. 7*. Tokyo: National Institute of Polar Research, pp. 122–132.

Paquette, J.-L., Nédélec, A., Moine, B. & Rakotondrazafy, M. (1994). U–Pb, single zircon Pb-evaporation, and Sm–Nd isotopic study of a granulite domain in SE Madagascar. *Journal of Geology* **102,** 523–538.

Peucat, J. J., Vidal, P., Bernard-Griffiths, J. & Condie, K. C. (1989). Sr, Nd, and Pb isotopic systematics in the Archean low- to high-grade transition zone of southern India: syn-accretion vs post-accretion granulites. *Journal of Geology* **97,** 537–550.

Peucat, J. J., Mahabaleswar, B. & Jayananda, M. (1993). Age of younger tonalitic magmatism and granulitic metamorphism in the South Indian transition zone (Krishnagiri area); comparison with older Peninsular gneisses from the Gorur–Hassan area. *Journal of Metamorphic Geology* **11,** 879–888.

Pinna, P., Jourde, G., Calvez, J. Y. & Mroz, J. P. (1993). The Mozambique Belt in northern Mozambique: Neoproterozoic (1100–850 Ma) crustal growth and tectogenesis, and superimposed Pan-African (800–550 Ma) tectonism. *Precambrian Research* **62,** 1–59.

Priem, H. N. A., Boelrijk, N. A. I. M., Hebeda, E. H., Verdurmen, E. A. T., Verschure, R. H., Oen, I. S. & Westra, L. (1979). Isotopic age determinations on granitic and gneissic rocks from the Ubendian–Usagaran system in southern Tanzania. *Precambrian Research* **9,** 227–239.

Quennell, A. M. (1960). Summary of the geology of Tanganyika, Part 2: Geological map. *Memoirs of the Geological Survey of Tanganyika* **1**.

Raase, P. & Schenk, V. (1994). Petrology of granulite-facies metapelites of the Highland Complex, Sri Lanka: implications for the metamorphic zonation and the *P–T* path. *Precambrian Research* **66,** 265–294.

Richard, P., Shimizu, N. & Allègre, C. J. (1976). $^{143}Nd/^{144}Nd$, a natural tracer: an application to oceanic basalt. *Earth and Planetary Science Letters* **31,** 269–278.

Robertson, D. K. (1973). A model discussing the early history of the Earth based on a study of lead isotope ratios from veins in some Archean cratons of Africa. *Geochimica et Cosmochimica Acta* **37,** 2099–2124.

Sampson, D. N. & Wright, A. E. (1964). The geology of the Uluguru Mountains. *Bulletin of the Geological Survey of Tanganyika* **37**.

Santosh, M., Kagami, H., Yoshida, M. & Nanda-Kumar, V. (1992). Pan-African charnockite formation in East Gondwana: geochronologic (Sm–Nd and Rb–Sr) and petrogenetic constraints. *Bulletin of the Indian Geological Association* **25,** 1–10.

Shackleton, R. M. (1967). Complex history of the Mozambique Belt. *Annual Reports on Scientific Results, University of Leeds* **11,** 12–13.

Shiraishi, K. & Kagami, H. (1992). Sm–Nd and Rb–Sr ages of metamorphic rocks from the Sør Rondane Mountains, East Antarctica. In: Yoshida, Y. (ed.) *Recent Progress in Antarctic Earth Science.* Tokyo: Terra, pp. 29–35.
Shiraishi, K., Ellis, D. J., Hiroi, Y., Fanning, C. M., Motoyoshi, Y. & Nakai, Y. (1994). Cambrian orogenic belt in East Antarctica and Sri Lanka: implications for Gondwana assembly. *Journal of Geology* **102**, 47–65.
Shiraishi, K., Kagami, H. & Yanai, K. (1995). Sm–Nd and Rb–Sr isochron ages for meta-trondhjemites from Cape Hinode, East Antarctica. *Proceedings of the NIPR Symposium, Vol. 8.* Tokyo: National Institute of Polar Research, pp. 130–136.
Stacey, J. S. & Kramers, J. D. (1975). Approximation of terrestrial lead isotope evolution by a two-stage model. *Earth and Planetary Science Letters* **26,** 207–221.
Stacey, J. S. & Stoeser, D. B. (1983). Distribution of oceanic and continental leads in the Arabian–Nubian shield. *Contributions to Mineralogy and Petrology* **84,** 91–105.
Stacey, J. S., Doe, B. R., Roberts, R. J., Delvaux, M. H. & Gramlich, J. W. (1980). A lead isotope study of mineralization in the Saudi Arabian shield. *Contributions to Mineralogy and Petrology* **74,** 175–188.
Stern, R. J. (1994). Arc assembly and continental collision in the Neoproterozoic East African Orogen: implications for the consolidation of Gondwanaland. *Annual Reviews of Earth and Planetary Sciences* **22,** 319–351.
Stern, R. J. & Dawoud, A. S. (1991). Late Precambrian (740 Ma) charnockite, enderbite, and granite from Jebel Moya, Sudan: a link between the Mozambique Belt and the Arabian–Nubian Shield? *Journal of Geology* **99,** 648–659.
Tanaka, T., Nakajima, T. & Shiraishi, K. (1985). Sm–Nd ages on the metamorphic rocks from Skarvsnes, East Antarctica (in Japanese). *6th Symposium on Antarctic Geosciences, NIPR Tokyo.* Tokyo: National Institute of Polar Research, p. 20.
Taylor, S. R. & McLennan, S. M. (1985). *The Continental Crust: Its Composition and Evolution.* Oxford: Blackwell.
Tilton, G. R., Pollack, R. J., Clark, A. H. & Robertson, R. C. R. (1981). Isotopic composition of Pb in Central Andean ore deposits. *Geological Society of America, Memoir* **154,** 791–816.
Todt, W., Cliff, R. A., Hanser, A. & Hofmann, A. W. (1996). Evaluation of a ^{202}Pb–^{205}Pb double spike for high-precision lead isotope analysis. In: Basu, A. & Hart, S. R. (eds) *Earth Processes: Reading the Isotopic Code.* Washington, DC: American Geophysical Union, pp. 429–437.
Unnikrishnan-Warrier, C., Santosh, M. & Yoshida, M. (1995). First report of Pan-African Sm–Nd and Rb–Sr mineral isochron ages from regional charnockites of southern India. *Geological Magazine* **132,** 253–260.
Watson, J. (1976). Vertical movements in Proterozoic structural provinces. *Philosophical Transactions of the Royal Society of London, Series A* **280,** 620–640.
Wendt, I., Besang, C., Harre, W., Kreuzer, H., Lenz, H. & Müller, P. (1972). Age determinations of granitic intrusions and metamorphic events in the Early Precambrian of Tanzania. *Proceedings 24th International Geological Congress,* pp. 295–314.
White, W. M. & Patchett, P. J. (1984). Hf–Nd–Sr isotopes and incompatible element abundances in island arcs: implications for magma origins and crust–mantle evolution. *Earth and Planetary Science Letters* **67,** 167–185.
Windley, B. F., Razafiniparany, A., Razakamanana, T. & Ackermand, D. (1994). Tectonic framework of the Precambrian of Madagascar and its Gondwana connections: a review and reappraisal. *Geologische Rundschau* **83,** 642–659.
Zhao, J. X., Shiraishi, K., Ellis, D. J. & Sheraton, J. W. (1995). Geochemical and isotopic studies of syenites from the Yamoto Mountains, East Antarctica: implications for the origin of syenitic magmas. *Geochimica et Cosmochimica Acta* **59,** 1363–1382.

APPENDIX A: ANALYTICAL METHODS

Mineral separation and isotope analysis procedures

K-feldspar and plagioclase were separated using standard procedures. Rock samples were crushed with a steel jaw-crusher and steel roller-mill or disk-mill to <0·5 mm. An appropriate size fraction was sifted off and the sample was washed with distilled water to remove surface dust. Feldspars were then concentrated using a Fronts Isodynamic Separator and heavy liquids before being hand-picked under a binocular microscope.

K-feldspar or plagioclase separates were leached in three steps. In the first step the feldspars were boiled overnight in aqua regia on a hot-plate. In the second step the samples were leached with a mixture of dilute HF and HNO_3 for 5–10 min on a hot-plate. In the last leaching step a stronger mixture of HF and HNO_3 was used until it resulted in visible size reduction of the K-feldspar grains. Plagioclase may appear not to dissolve because of the precipitation of CaF_2, which mimics the original grains. Between each step the samples were washed with pure H_2O. Final dissolution was achieved with concentrated HF [see also DeWolf & Mezger (1994)].

Pb was separated on Teflon columns filled with about 0·5 ml of Dowex AG1 × 8 anion exchange resin using the HBr–HCl method (Krogh, 1973). For isotope analysis Pb was loaded with phosphoric acid and silica gel (Cameron *et al.*, 1969) on single Re filaments. Isotope ratios were measured on a Finnigan MAT 261 mass spectrometer in multi-collector static mode. The measured Pb isotopic ratios were corrected for mass discrimination with a factor of 0·1% per a.m.u. (atomic mass unit) based on 23 repeat analyses of 50 ng of NBS equal atom standard SRM NBS-982, measured throughout the duration of the study. Mass discrimination was determined relative to the measurements of Todt *et al.* (1996), which were obtained on the same mass-spectrometer with the same silica gel as used for loading. Standards were measured in the same temperature range as samples, between 1270°C and 1400°C. Reproducibility of the ^{207}Pb/^{206}Pb ratio of the standard was 0·033%. Mean within-run uncertainty was on average 0·002%. Five total procedural blanks for Pb were determined, and ranged from 44 to 123 pg with an average of 80 pg. The Pb isotope ratios measured for the blank were: ^{206}Pb/^{204}Pb, 18·53; ^{207}Pb/^{204}Pb, 15·69; ^{208}Pb/^{204}Pb, 35·90.

For analysis of Rb–Sr and Sm–Nd, rock samples were crushed with a steel jaw-crusher and splits reduced to powder in an agate shatterbox. Before dissolution the sample powders were dried for 24 h at 110°C. An $^{149}Sm/^{150}Nd$ mixed spike was added and the samples were then digested in several steps. The first step involved 1 ml of concentrated HF in a closed 3 ml Savilex screw-top beaker on a hot-plate overnight and drying afterwards to reduce the sample size by driving off silica. The second step was conducted with 1 ml of concentrated HF and about five drops of 7N HNO_3 in a Krogh-style Teflon bomb within a screw-top steel container, which was placed in an oven at 210°C for 5–7 days. To break down fluorides, concentrated $HClO_4$ was added to the samples and then dried on a hot-plate. Residual $HClO_4$ was driven off with HCl.

Sm, Nd and Sr were separated using a method modified from White & Patchett (1984). For the separation of Sr and REE as a group, columns filled with about 50 ml of Dowex AG 50WX12 resin were used. Sm and Nd were separated with 5 ml Teflon columns coated with hydrogen-diethylhexyl-phosphate (HDEHP) (Richard *et al.*, 1976).

Isotope ratios were measured on a Finnigan MAT 261 mass spectrometer in multi-collector static mode for Sm, Nd and Sr. Double Re filaments were used for Sm and Nd measurements, single W filaments with TaF_5 for Sr. The mean $^{143}Nd/^{144}Nd$ ratio obtained on repeated analyses of the La Jolla standard during the study was 0·511842 ± 20 (n = 13). Fractionation was corrected by normalizing the isotope ratios to $^{146}Nd/^{144}Nd$ = 0·7219. Sm/Nd ratios were determined to a precision of ~0·2%. A total procedural blank for Nd was determined at 340 pg and is negligible, because Nd content of the samples is higher by a factor of ~2000.

Rb and Sr concentrations were obtained from X-ray fluorescence, and ICP-MS for low concentrations [see also Appel (1996)]. The errors for concentrations and for the calculated $^{87}Rb/^{86}Sr$ ratios are in the range of 2–5%. Thirteen runs of the NBS 987 standard yielded a mean $^{87}Sr/^{86}Sr$ value of 0·710208 ± 18 (n = 13). Fractionation was corrected by normalizing the ratios to $^{86}Sr/^{88}Sr$ = 0·1194. All errors for isotope results are given as $2\sigma_m$.

Data reproducibility and model age error evaluation

The precision of the model age determinations is a major controlling factor for the validity of the interpretations of such ages in terms of apparent crustal residence ages and their geological significance. Reproducibility based on duplicate dissolutions of samples (Table 1) is usually better than 0·4 ε_{Nd} units, except for a metapelite sample unusually rich in the REE-bearing mineral monazite, which reproduces only to within 2·7 ε_{Nd} units (A108G). This difference, however, is nearly outweighed by different $^{147}Sm/^{144}Nd$ ratios of the duplicates that yield model ages differing by <40 my. The average difference in the $^{147}Sm/^{144}Nd$ ratios of duplicate solutions is 0·006. Thus, Nd model ages of the duplicates can be reproduced to within 55 my on average. However, the span of age differences between 4 Ma and 118 Ma indicates that it is not useful to discuss Nd model age differences on a scale of less than 100 my. The reproducibility of duplicate analyses from the same solution (Table 1) is also in the range of 0·1–0·8 ε_{Nd} units, comparable with the difference between separate dissolutions. Within-run precision is better than 0·4 ε_{Nd} units for all but one of the measurements, and on average better than 0·2 ε_{Nd} units.

The accuracy of the Sr model ages calculated is partly limited by the error on the $^{87}Rb/^{86}Sr$ ratio, which is estimated from the error on the measurement of Rb by XRF and/or ICP-MS. For those samples with very low Rb concentrations, however, the error is almost insignificant, because any calculation with the resulting very low Rb/Sr ratio leads to geologically meaningless ages.

The reproducibility of the Sr isotopic composition between runs of 0·0011% is identical to the within-run error (resulting in an average difference in Sr model age of only ±2 Ma) and both are thus insignificant in the error estimate on Sr model ages because they are so much better than the uncertainty of the Rb/Sr ratio. Reproducibility between different solutions prepared from the same sample resulted in an average difference in Sr model age of only ±9 Ma. On the other hand, an error of 5% on the Rb/Sr typically results in an uncertainty of about ±150 Ma on a 2500 Ma Sr model age. It follows that the uncertainty of Sr model age calculation largely rests on the determination of the Rb/Sr ratio and the uncertainty of mantle models for Sr isotopic evolution.

APPENDIX B: CENTRAL GONDWANA Nd MODEL AGES

Table B1: Compilation of Sm–Nd isotopic data from central Gondwana

Sample	Rock type	$^{143}Nd/^{144}Nd$	$^{147}Sm/^{144}Nd$	ε_{Nd} T_0	$T_{DM}G^a$ (Ma)	Correct. $T_{DM}G$ (Ma)	Tcorr (Ga)	Sm (ppm)	Nd (ppm)
Maboko & Nakamura (1996), Tanzania									
Usagaran									
IRA 1	foliated granite	0·511032	0·0773	−31·3	**2362**			5·30	41·28
IRA2	foliated granite	0·511066	0·0879	−30·7	**2518**			4·50	30·82
IRA 3	Ilula granite	0·511013	0·0770	−31·7	**2378**			3·45	26·58
IRA 4	Ilula granite	0·511213	0·0990	−27·8	**2567**			18·30	110·20
IRA 6	Ilula granite	0·511219	0·0980	−27·7	**2537**			13·00	79·84
IRA 7	Ilula granite	0·511144	0·0908	−29·1	**2482**			12·50	82·88
IRA 8	probably Ilula granite	0·511124	0·0845	−29·5	**2385**			3·96	27·77
IRA 9	foliated granite	0·510996	0·0764	−32·0	**2386**			5·23	40·95
IRA 10	fine-grained granite	0·510951	0·0871	−32·9	**2639**			2·91	20·04
IRA 21	unfoliated granite	0·511274	0·1091	−26·6	**2725**			7·81	43·02
IRA 11	deformed granite	0·511197	0·1133	−28·1	**2952**			36·00	191·04
Craton									
IRA 12	highly deformed granite	0·510928	0·0947	−33·4	**2834**			1·20	7·56
IRA 14	amphibolite	0·511427	0·1227	−23·6	**2875**			11·00	53·84
IRA 17	granite, low-grade met.	0·510682	0·0810	−38·2	**2823**			1·13	8·17
IRA 19	highly def. met. granite	0·510884	0·0929	−34·2	**2847**			5·75	36·92
IRA 24	granitic gneiss	0·510578	0·0878	−40·2	**3097**			1·67	11·65
IRA 25	granitic gneiss	0·511491	0·1238	−22·4	**2803**			2·83	13·62
Maboko (1995), Tanzania									
WAM1	Wami granulite	0·512501	0·1290	−2·7	**1181**			3·62	16·89
MOR1	Bt–Hbl gneiss	0·511715	0·1361	−18·0	**2810**			3·28	14·51
MOR2	Mindu Mt granitic gn.	0·511121	0·1056	−29·6	**2849**			2·80	15·96
MOR3	locality not described	0·511232	0·1035	−27·4	**2645**			6·30	36·69
MOR6	Uluguru granulite	0·512041	0·1248	−11·6	**1906**			3·46	16·68
MOR8	Ulug. anorthosite	0·512215	0·1291	−8·3	**1693**			2·09	9·74
MOR9	Ulug. anorthosite	0·512138	0·1142	−9·8	**1558**			1·07	5·65
MOR10	Ulug. anorthosite	0·511758	0·0960	−17·2	**1806**			2·80	17·53
MOR14	Ulug. granulite	0·512145	0·1456	−9·6	**2252**			2·68	11·08
MOR16	Ulug. granulite	0·511511	0·1046	−22·0	**2288**			5·17	29·74
MOR17	Ulug. granulite	0·512225	0·1493	−8·1	**2194**			0·72	2·90
DOM1	Craton, migm. Bt gn.	0·510409	0·0733	−43·5	**2961**			3·51	28·80
DOM4	Mpwapwa Bt gn.	0·510788	0·0898	−36·1	**2893**			3·04	20·38
DOM5	Mpwapwa Bt gn.	0·510674	0·0735	−38·3	**2682**			3·39	27·77
Ben Othman et al. *(1984), East Africa*									
Tz7051	Msagali charnockite	0·511310	0·1260	−25·9	**3181**			1·82	8·62
Ug 7012	aplitic granulite	0·510570	0·0794	−40·3	**2914**			0·39	2·97
Ug 7020	Western Nile complex	0·510770	0·1164	−36·4	**3699**			3·00	15·58
Ind 7217	basic charnockite		0·1957					1·61	4·99
Ind 7246	charnockite	0·512060	**0·1572**	−11·3	**2933**	2762	2·5	3·48	13·37
Harris et al. *(1984), Kenya*									
K 34	Marich granite	0·512020	0·1220	−12·1	**1883**			0·48	2·38

Sample	Rock type	$^{143}Nd/^{144}Nd$	$^{147}Sm/^{144}Nd$	ε_{Nd} T_0	$T_{DM}G^a$ (Ma)	Correct. $T_{DM}G$ (Ma)	Tcorr (Ga)	Sm (ppm)	Nd (ppm)
K 35	Marich granite	0·511850	0·1230	−15·4	**2185**			0·21	1·03
K 32	Metapelite Sekerr	0·512390	0·1270	−4·8	**1347**			1·33	6·33
K 33	Metapelite Sekerr	0·512370	0·1270	−5·2	**1382**			1·09	5·17
K 57B	Amphibolite Sekerr	0·512430	0·1200	−4·1	**1183**			5·60	28·20
Key et al. *(1989), Kenya*									
CRK/b	Il Poloi granite	0·512802	**0·1625**	3·2	**1059**	874	0·65	5·92	22·02
CRK/e	Il Poloi granite	0·512740	**0·1647**	2·0	**1297**	990	0·65	3·88	14·24
Milisenda et al. *(1994), Sri Lanka*									
SL 8.3	Highland Complex	0·511217	0·1130	−27·7	**2914**			11·56	61·84
PR 22		0·511283	0·1186	−26·4	**2979**			8·30	42·27
PR 41		0·511285	0·1134	−26·4	**2824**			17·98	95·83
SL 45		0·511521	0·1069	−21·8	**2322**			6·56	37·08
SL 57		0·511561	0·1086	−21·0	**2302**			3·83	21·30
SL 62		0·511165	0·1093	−28·7	**2886**			10·04	55·51
SL 82		0·511316	0·1102	−25·8	**2693**			6·13	33·62
SL 98		0·511341	0·1079	−25·3	**2599**			1·62	9·09
SL 110		0·511933	**0·1702**	−13·8	**4225**	2300	0·6	9·86	35·04
SL 125		0·511196	0·1109	−28·1	**2885**			5·43	29·61
SL 137		0·511302	0·1373	−26·1	**3660**			16·72	73·58
K 200-10		0·511272	0·1110	−26·6	**2777**			9·89	54·33
K 200-2A		0·511263	0·0945	−26·8	**2408**			6·80	43·47
K 320-1		0·511292	0·1090	−26·3	**2696**			9·28	51·52
1038		0·511089	0·0860	−30·2	**2454**			7·57	53·18
1039		0·511095	0·0864	−30·1	**2455**			8·76	61·27
K 339		0·512004	0·1300	−12·4	**2090**			9·06	42·20
SL 349		0·511348	0·0824	−25·2	**2091**			9·40	61·93
SL 351		0·511302	0·1130	−26·1	**2787**			10·83	58·07
SL 351-1C		0·511285	0·0843	−26·4	**2195**			2·64	18·59
SL 351-2		0·511300	0·0959	−26·1	**2389**			7·87	49·56
SL 355		0·511083	0·0925	−30·3	**2592**			7·62	49·83
SL 357		0·511233	0·0974	−27·4	**2506**			5·65	35·06
SL 410		0·510981	0·1020	−32·3	**2946**			21·64	127·70
SL 669		0·511116	0·0905	−29·7	**2510**			12·23	81·67
SL 794		0·511165	0·1089	−28·7	**2875**			8·29	45·98
SL 397		0·511245	0·1150	−27·2	**2929**			9·01	47·34
SL 402		0·512023	**0·1885**	−12·0	**6670**	2271	0·6	8·53	27·37
K 418		0·511930	**0·1510**	−13·8	**2957**	2183	0·6	20·60	82·50
K 419		0·511240	0·1140	−27·3	**2908**			8·91	47·50
K 408	Vijayan	0·511468	0·1050	−22·8	**2355**			2·65	15·25
SL 38		0·512224	0·1060	−8·1	**1319**			5·60	31·93
SL 66		0·512289	0·1248	−6·8	**1486**			5·31	25·72
SL 164		0·512247	0·1141	−7·6	**1391**			5·62	29·77
SL 359		0·512261	0·1270	−7·4	**1572**			4·26	20·18

Table B1: continued

Sample	Rock type	$^{143}Nd/^{144}Nd$	$^{147}Sm/^{144}Nd$	ε_{Nd} T_0	$T_{DM}G^a$ (Ma)	Correct. $T_{DM}G$ (Ma)	Tcorr (Ga)	Sm (ppm)	Nd (ppm)
SL 359-3A		0·512222	0·0953	−8·1	**1204**			3·96	25·15
SL 359-3B		0·512190	0·0804	−8·7	**1106**			4·48	33·66
SL 359-3C		0·512459	0·1290	−3·5	**1256**			4·64	21·76
SL 359-3D		0·512603	0·1330	−0·7	**1048**			2·84	12·89
SL 359-3E		0·512439	0·1110	−3·9	**1067**			3·07	16·79
SL 359-3F		0·512527	0·1330	−2·2	**1190**			4·20	19·12
SL 359-3G		0·512562	0·1360	−1·5	**1168**			1·14	5·06
SL 362		0·512281	0·1203	−7·0	**1428**			5·26	26·45
SL 391		0·512668	**0·1555**	0·6	**1281**	1024	0·6	2·33	9·04
SL 403		0·512126	0·1307	−10·0	**1886**			1·32	6·11
SL 584		0·512239	0·1324	−7·8	**1716**			2·28	10·03
SL 587		0·512498	0·1327	−2·7	**1240**			4·87	22·20
SL 611		0·512156	0·1131	−9·4	**1514**			9·59	51·22
SL 613		0·512421	0·1295	−4·2	**1331**			3·86	18·01
SL 616	Wanni	0·512320	0·1199	−6·2	**1359**			8·49	42·78
SL 18		0·512150	0·1224	−9·5	**1677**			8·55	42·22
SL 29		0·511795	0·0891	−16·4	**1662**			2·96	20·10
SL 30		0·511738	0·0867	−17·6	**1699**			5·46	38·08
SL 56		0·511954	0·1177	−13·3	**1903**			3·85	19·76
SL 414		0·511948	0·1063	−13·5	**1711**			5·71	32·48
SL 68		0·511622	0·0888	−19·8	**1867**			9·39	63·94
SL 71		0·512138	0·1139	−9·8	**1553**			3·91	20·78
SL 277-4a		0·511840	0·0946	−15·6	**1681**			8·66	55·31
SL 277-4c		0·511776	0·0820	−16·8	**1595**			4·30	31·69
SL 542		0·511794	0·1104	−16·5	**2003**			8·75	47·94
SL 544		0·511795	0·1087	−16·4	**1969**			3·21	17·88
SL 325		0·512137	0·1221	−9·8	**1693**			6·64	32·88
SL 330		0·512303	0·1323	−6·5	**1596**			9·36	42·76
SL 332		0·512099	0·1190	−10·5	**1698**			6·21	31·54
SL 333		0·512156	0·1034	−9·4	**1382**			9·54	55·81
SL 336		0·511828	0·1176	−15·8	**2098**			2·32	11·91
SL 339		0·511937	0·1030	−13·7	**1675**			20·07	117·20
SL 348		0·512395	0·1448	−4·7	**1681**			4·87	20·34
SL 417		0·512333	0·1391	−5·9	**1679**			10·75	46·71
SL 442		0·512264	0·1310	−7·3	**1642**			5·05	23·26
SL 460		0·511839	0·0897	−15·6	**1616**			5·08	34·24
SL 622		0·512175	0·1166	−9·0	**1539**			2·88	14·91
SL 648		0·512139	0·1093	−9·7	**1484**			4·39	24·27
SL 706		0·512315	0·1372	−6·3	**1673**			5·80	25·55
SL 708		0·512610	**0·1632**	−0·5	**1647**	1166	0·6	3·23	11·96
SL 789		0·512185	0·1146	−8·8	**1493**			6·92	36·51
SL 1		0·512166	0·1243	−9·2	**1685**			6·59	32·07
SL 2.1		0·512273	0·1254	−7·1	**1523**			13·43	64·72
SL 5.1		0·512207	0·1178	−8·4	**1507**			17·73	90·98

Sample	Rock type	$^{143}Nd/^{144}Nd$	$^{147}Sm/^{144}Nd$	ε_{Nd} T_0	$T_{DM}G$[a] (Ma)	Correct. $T_{DM}G$ (Ma)	Tcorr (Ga)	Sm (ppm)	Nd (ppm)
Kagami et al. *(1990), Sri Lanka, Highland Complex*									
2153		0·511437	0·1196	−23·4	**2766**			6·64	33·6
2154-0		0·511341	0·1134	−25·3	**2740**			20·5	109
2154-1		0·511654	0·1336	−19·2	**2838**			10·6	48·0
2154-2		0·511077	0·0960	−30·5	**2676**			7·01	44·1
2157-0		0·511345	0·1120	−25·2	**2697**			8·26	44·6
2157-1		0·511189	0·0633	−28·3	**1987**			17·9	170
2157-2		0·511223	0·1119	−27·6	**2874**			46·1	249
2157-3		0·511180	0·1140	−28·4	**2998**			12·8	67·7
2157-4		0·511147	0·1122	−29·1	**2994**			4·06	21·9
Burton & O'Nions (1990),[b] *Sri Lanka, Vijayan, normalized to 0·7219*									
222		0·511839	0·1002	−15·6	**1765**			7·60	45·81
220-0		0·511843	0·1010	−15·5	**1772**			7·89	47·20
220-6		0·511748	0·0752	−17·4	**1548**			5·75	46·21
221		0·511804	0·0857	−16·3	**1608**			7·22	50·94
Paquette et al. *(1994), SE Madagascar, Androyan complex*									
A 1002		0·511069	0·0774	2·32	**2323**			1·58	12·35
A 1010		0·511500	0·0966	2·14	**2147**			3·02	18·89
A 1111		0·511257	0·0940	2·40	**2406**			6·32	40·58
A 1118		0·511199	0·1076	2·79	**2792**			11·87	66·62
A 1131		0·511249	0·1054	2·66	**2667**			7·04	40·34
A 1210		0·510897	0·0762	2·49	**2491**			17·06	135·13
Unnikrishnan-Warrier et al. *(1995), S India, Trivandrum, normalized to 0·7219*									
Kottaram	massive charnockite	0·510875	0·0640		**2323**			6·58	61·91
Choudhary et al. *(1992), S India, Trivandrum*									
C10a	charnockite	0·511340	0·1024	2·68	**2474**			11·85	69·93
G11	amphib. facies gneiss	0·511190	0·1149	2·35	**3010**			12·39	65·18
C15a	charnockite	0·511170	0·0995	2·30	**2635**			12·62	76·61
G15a	amphib. facies gneiss	0·511180	0·1162	2·69	**3065**			13·78	71·67
C15b	charnockite	0·511150	0·1067	2·64	**2838**			14·30	80·98
Harris et al. *(1994), S India, normalized to 0·7219*									
Palgat–Cauvery shear zone									
KKD-A	incipient charnockites	0·511535	0·1094	−21·5	**2357**			5·64	31·13
KKD-B		0·511311	0·0950	−25·9	**2358**			4·29	27·30
WA3	gneiss or metapelite	0·512067	0·1352	−11·1	**2106**			1·61	7·20
Western Madurai Block, south of P.–C.									
327	massive charnockites	0·511364	0·1122	−24·9	**2674**			2·70	12·24
PE5		0·511068	0·1035	−30·6	**2868**			7·29	42·53
VD4		0·511575	0·1163	−20·7	**2461**			8·69	45·19
33		0·511002	0·0946	−31·9	**2739**			3·92	25·06
104		0·511314	0·1114	−25·8	**2727**			9·53	51·70
VD1	alkali granite	0·511353	0·0886	−25·1	**2188**			1·00	6·84
Trivandrum Block									
27A	incipient charnockites	0·511317	0·1139	−25·8	**2790**			13·74	72·92

Table B1: continued

Sample	Rock type	$^{143}Nd/^{144}Nd$	$^{147}Sm/^{144}Nd$	ε_{Nd} T_0	$T_{DM}G^a$ (Ma)	Correct. $T_{DM}G$ (Ma)	Tcorr (Ga)	Sm (ppm)	Nd (ppm)
27B		0·511257	0·0921	−26·9	**2369**			10·74	70·50
28A		0·511342	0·1075	−25·3	**2588**			14·37	80·81
28B		0·511454	0·0894	−23·1	**2079**			12·50	84·52
34A	massive charnockite	0·511353	0·0886	−25·1	**2188**			7·33	49·96
17A	gneisses + metapelites	0·511363	0·1417	−24·9	**3754**			7·86	33·51
19A		0·512211	0·1253	−8·3	**1627**			5·57	26·87
19B		0·512197	0·1189	−8·6	**1541**			6·67	33·89
21A		0·511379	0·1108	−24·6	**2616**			2·60	14·16
21C		0·511436	0·1434	−23·4	**3689**			5·79	24·43
24A		0·511811	0·1242	−16·1	**2280**			3·31	16·12
25B		0·511219	0·1052	−27·7	**2704**			10·93	60·86
30A		0·511169	0·1031	−28·7	**2721**			14·09	82·63
32A		0·511353	0·1140	−25·1	**2738**			17·94	95·19
32D		0·511318	0·1200	−25·7	**2967**			78·33	394·58
32F		0·511155	0·0942	−28·9	**2538**			115·31	740·27
35B		0·511303	0·1185	−26·0	**2945**			10·71	54·62
Karnataka Craton, north of P.–C.									
EM	massive charnockite	0·510742	0·1067	−37·0	**3407**			2·49	14·09
Santosh et al. *(1992), S India, south of P.–C.*									
NL/86/B	Crd charnockite	0·511861	0·0920	−15·2	**1619**			4·05	25·69
0103B	Crd charnockite	0·512140	0·1187	−9·7	**1628**			7·87	38·70
Bernhard-Griffiths et al. *(1987), S India, north of P.–C.*									
5590	acid charnockites	0·510824	0·0853	−35·4	**2750**			5·13	36·34
5592		0·511177	0·1056	−28·5	**2772**			6·28	41·89
5594		0·510871	0·0906	−34·5	**2810**			3·14	17·98
5589	basic	0·511537	0·1258	−21·5	**2788**			4·97	18·32
5595		0·512744	**0·1970**	2·1	**3697**	2758	2·55	2·83	13·60
5596		0·512045	**0·1640**	−11·6	**3372**	2988	2·55	3·04	9·33
5593	ultrabasic	0·511139	0·1047	−29·2	**2801**			4·28	24·71
5591	leptynite	0·512031	**0·1577**	−11·8	**3036**	2841	2·55	1·44	5·52
Drury et al. *(1983), India, north of P.–C., normalized to 0·7219*									
KT10	Karnataka craton	0·511622	0·1424	−19·8	**3250**			4·52	19·19
KT14	metavolcanics	0·511801	**0·1516**	−16·3	**3294**	3045	2·55	3·12	12·45
KT19		0·511786	**0·1505**	−16·6	**3273**	3039	2·55	1·55	6·22
Peucat et al. *(1989), India, Karnataka, north of P.–C., normalized to 0·7219*									
6697	TZ, tonalitic gneisses	0·511152	0·1059	−29·0	**2814**			3·12	17·81
6603		0·511006	0·0948	−31·8	**2738**			1·92	17·21
6604		0·510937	0·0905	−33·2	**2728**			1·66	11·07
6606		0·510556	0·0678	−40·6	**2699**			0·52	4·59
6610	TZ, granitic gneisses	0·510691	0·0769	−38·0	**2729**			4·40	34·57
6611	average of 2	0·510335	0·0523	−44·9	**2648**			0·19	2·22
6612		0·510711	0·0778	−37·6	**2725**			1·81	14·09
6615		0·510576	0·0685	−40·2	**2692**			1·33	11·73
6617	TZ, low-*P* charnockites	0·510506	0·0664	−41·6	**2725**			4·13	37·62
6620		0·510678	0·0732	−38·2	**2672**			2·11	17·41

Sample	Rock type	$^{143}Nd/^{144}Nd$	$^{147}Sm/^{144}Nd$	ε_{Nd} T_0	$T_{DM}G$[a] (Ma)	Correct. $T_{DM}G$ (Ma)	Tcorr (Ga)	Sm (ppm)	Nd (ppm)
6621		0·511020	0·1003	−31·6	**2851**			4·38	26·41
6622		0·511280	0·1121	−26·5	**2795**			8·99	48·52
6623		0·510491	0·0671	−41·9	**2753**			0·83	7·46
6624		0·511041	0·0996	−31·2	**2806**			1·33	8·09
8137	high-*P* charn., BR hills	0·510769	0·0852	−36·5	**2812**			2·96	21·00
8138	BR hills	0·510377	0·0707	−44·1	**2941**			1·29	0·11
8139	Nilgiri Block	0·511432	0·1251	−23·5	**2944**			3·78	18·26
Peucat et al. *(1993), India, Karnataka, north of P.–C., normalized to 0·7219*									
Ind 55b	Hassan Gorur	0·511591	0·1456	−20·4	**3468**			1·44	5·98
Ind 55d		0·511835	**0·1562**	−15·7	**3466**	3114	2·55	13·95	53·99
Gor 3a2		0·512028	**0·1653**	−11·9	**3514**	3050	2·55	11·98	43·83
Gor 3b		0·510783	0·1065	−36·2	**3344**			4·86	27·59
HL1a		0·511253	0·1297	−27·0	**3420**			4·29	19·99
HL5a	Halekote	0·511393	0·1348	−24·3	**3374**			1·90	8·50
Ind 56a	Segegudda	0·511441	0·1360	−23·3	**3333**			9·92	44·08
Brandon & Meen (1995), S India, Trivandrum									
35-71	Kerala Grt–Bt gneiss	0·511185	0·0980	−28·3	**2581**			13·65	84·22
33-64	Grt–Bt gneiss	0·511234	0·1137	−27·4	**2908**			12·72	67·67
125-174	Grt–Bt gneiss	0·511145	0·0969	−29·1	**2609**			18·45	115·2
49-87	Grt–Bt gneiss	0·510850	0·0843	−34·9	**2699**			7·06	50·27
25-56	Grt–Bt gneiss	0·511491	0·1101	−22·4	**2437**			2·37	13·02
83-124a	Grt–Bt gneiss	0·511262	0·0922	−26·8	**2364**			28·49	186·9
63-97	Grt–Bt gneiss	0·511185	0·0756	−28·3	**2167**			22·47	179·7
16-34	Khond	0·511696	0·1309	−18·4	**2670**			8·29	38·30
77-115	Crd gneiss	0·512162	0·1046	−9·3	**1389**			9·88	57·12
91-133	Cardamom enderbite	0·511588	0·0833	−20·5	**1828**			14·63	106·3
100-140	charnockite	0·511392	0·1015	−24·3	**2384**			9·41	56·06
101-141	enderbite	0·511351	0·1111	−25·1	**2665**			7·32	39·88
103-144	enderbite	0·511436	0·1153	−23·4	**2648**			7·95	41·73
184-274	charnockite	0·511147	0·1008	−29·1	**2695**			7·69	46·44
Jayananda et al. *(1995), S India, Madurai, Kodaikanal Complex*									
KOK 18	charnockite	0·511218	0·1144	−27·7	**2953**			3·81	20·14
US 25	charnockite	0·511265	0·0926	−26·8	**2368**			5·19	33·54
US 31	charnockite	0·511393	0·1313	−24·3	**3233**			7·98	37·01
KOD5	charnockite	0·511029	0·1048	−31·4	**2955**			7·30	42·10
P 6-2	mafic granulite	0·512157	**0·1633**	−9·4	**2995**	1919	0·65	2·29	8·52
OD22	anorthosite	0·511485	0·1097	−22·5	**2436**			0·13	0·71
P 4-1	charnockite	0·511241	0·1227	−27·3	**3181**			8·07	39·74
Bhaskar Rao et al. *(1996), S India, Sittampundi Complex*									
92SLM-84	meta-anorthos. gabbro	0·51206	0·1189	−11·3	**1758**			3·5	18·1
92SLM-85	metagabbroic anorthos.	0·51122	0·1183	−27·7	**3069**			4·6	23·5
94SLM-7	metagabbroic anorthos.	0·51127	0·1195	−26·7	**3028**			4·0	20·5
94SLM-41	metapyroxenite	0·51162	0·1394	−19·9	**3124**			0·1	0·3
94SLM-42	metapyroxenite	0·51197	**0·1591**	−13·0	**3279**	3163	3·0	1·3	4·9
94SLM-26	Grt metagab. anorthos.	0·51216	**0·1685**	−9·3	**3324**	3157	3·0	0·2	0·6

Table B1: continued

Sample	Rock type	$^{143}Nd/^{144}Nd$	$^{147}Sm/^{144}Nd$	ε_{Nd} T_0	$T_{DM}G^{a}$ (Ma)	Correct. $T_{DM}G$ (Ma)	Tcorr (Ga)	Sm (ppm)	Nd (ppm)
94SLM-15	meta-anorthosite	0·51227	**0·1739**	−7·2	**3357**	3152	3·0	0·1	0·4
92SLM-81	meta-anorthos. gabbro	0·51259	**0·1880**	−0·9	**3316**	3087	3·0	2·7	8·6
92SLM-77	Grt metagabbro	0·51284	**0·2006**	3·9	**3609**	3087	3·0	2·1	6·4
94SLM-13	meta-anorthos. gabbro	0·51284	**0·2024**	3·9	**4161**	3144	3·0	0·1	0·3
94SLM-58	Grt metagabbro	0·51288	**0·2051**	4·7	**4736**	3165	3·0	2·5	7·2
94SLM-50	Grt metagab. anorthos.	0·51369	**0·2436**	20·5	**2714**	not app.		0·1	0·3
92SLM-83	Grt metagabbro	0·51281	**0·2021**	3·4	**4432**	3182	3·0	2·4	7·5
92SLM-87	meta-anorthos. gabbro	0·51133	0·1237	−25·5	**3068**			0·7	3·5
South India, Bhavani Complex									
94BH-50	metagabbroic anorthos.	0·51123	0·1171	−27·5	**3016**			3·7	29·3
94BH-55	metagabbro	0·51123	0·1171	−27·5	**3016**			3·2	11·6
94BH-49	metagabbroic anorthos.	0·51254	**0·1858**	−1·9	**3325**	3098	3·0	0·4	1·2
94BH-57	Grt metagabbro	0·51278	**0·1980**	2·8	**3589**	3100	3·0	2·0	6·2
Black et al. *(1987), Antarctica, Rayner Complex*									
78285009	paragneiss	0·511976	0·1164	−12·9	**1844**			6·43	33·4
78285010	pegmatite	0·511591	0·1017	−20·4	**2121**			36·20	215
78285023	granitic orthogn.	0·511482	0·1091	−22·5	**2426**			6·26	34·7
78285024	granite	0·511262	0·0829	−26·8	**2198**			6·61	48·2
78285027	granitic orthogn.	0·511510	0·1103	−22·0	**2413**			3·82	20·9
80285043B	anorthositic layer	0·511492	0·0971	−22·4	**2166**			1·73	10·7
80285043M	gabbroic layer	0·511516	0·1074	−21·9	**2340**			1·43	8·00
80285049	granitic orthogn.	0·511373	0·1010	−24·7	**2399**			7·36	44·1
77283498	tonalitic orthogn.	0·512112	0·1435	−10·3	**2256**			2·92	12·3
77283554	granitic orthogn.	0·512127	0·1043	−10·0	**1433**			3·64	21·1
McCulloch & Black (1984), Antarctica, Enderby Land, Napier, min. age 3·8 Ga, poss. disturbed									
M	charnockite	0·509928	0·0694	−52·9	**3380**			1·81	15·72
N	charnockite	0·510158	0·0810	−48·4	**3413**			0·82	6·11
J1	charnockite	0·510589	0·0991	−40·0	**3384**			1·70	10·37
J5	charnockite	0·509968	0·0692	−52·1	**3334**			0·53	4·65
50	leuconorite	0·510188	0·0782	−47·8	**3310**			1·73	13·37
53	leuconorite	0·510769	0·1087	−36·5	**3433**			1·34	7·49
54	leuconorite	0·511120	0·1265	−29·6	**3525**			1·15	5·50
51	gabbro	0·511140	0·1296	−29·2	**3617**			10·05	46·92
56	gabbro	0·511470	0·1461	−22·8	**3759**			4·90	20·61
56b	gabbro	0·511550	0·1468	−21·2	**3691**			4·91	20·21
57	gabbro	0·510869	0·1113	−34·5	**3373**			5·49	29·84
Black et al. *(1986), Antarctica, Enderby Land, Napier Mts granites*									
80285032	granite	0·510519	0·09335	−41·3	**3311**				
80285033	granite	0·510999	0·11737	−32·0	**3381**				
77284670	granite	0·511480	0·14416	−22·6	**3634**				
Black & McCulloch (1987), Antarctica, Enderby Land, Napier, Mt Sones									
7683267	paragneiss	0·510759	0·1108	−36·7	**3517**			5·84	31·89
77283464	leucogneiss	0·510659	0·1001	−38·6	**3321**			1·10	6·27
77283465	grt-bearing gneiss	0·509727	0·0777	−56·8	**3803**			1·96	15·29
77283466	metapelite	0·515136	**0·3865**	48·7	**1742**	3882	2·5	61·61	96·39

Sample	Rock type	$^{143}Nd/^{144}Nd$	$^{147}Sm/^{144}Nd$	ε_{Nd} T_0	$T_{DM}G^a$ (Ma)	Correct. $T_{DM}G$ (Ma)	Tcorr (Ga)	Sm (ppm)	Nd (ppm)
77283467	tonalitic orthogneiss	0·511370	0·1499	−24·7	**4211**			6·66	26·87
78285007-A	tonalitic orthogneiss	0·509808	0·0865	−55·2	**3968**			3·49	24·42
78285007-F	tonalitic orthogneiss	0·509918	0·0901	−53·1	**3950**			4·36	29·24
78285007-J	tonalitic orthogneiss	0·509657	0·0785	−58·1	**3902**			3·97	30·64
78285008–9	paragneiss	0·511640	**0·7121**	−19·5	**−467**	6437	0·65	5·81	20·42
Arndt et al. *(1991), Antarctica, Heimefrontfjella*									
17.1/7	Grt amphibolite	0·512486	**0·1533**	−3·0	**1688**	1480	1·0	39·0	156
4.1/11	granitoids and	0·511996	0·0920	−12·5	**1452**			8·90	58·7
A7.1/1	orthogneisses	0·512112	0·0986	−10·3	**1382**			19·0	116
5.1/8		0·512128	0·1038	−9·9	**1425**			12·0	68·0
27.1/1		0·512229	0·1322	−8·0	**1730**			13·2	60·0
23.1/11		0·512166	**0·1573**	−9·2	**2657**	2041	1·0	0·50	2·00
25.2/9		0·512192	0·1301	−8·7	**1754**			21·9	101
2.2/5		0·512039	0·1007	−11·7	**1505**			14·0	82·0
9.2/22	charnockites	0·512177	0·1247	−9·0	**1674**			14·1	68·4
10.2/2		0·512070	0·1232	−11·1	**1825**			11·8	58·1
12.2/1		0·512319	0·1370	−6·2	**1661**			13·7	60·0
14.2-14		0·512059	0·1124	−11·3	**1648**			2·30	12·2
10.2/1	granulite	0·512192	0·1405	−8·7	**2001**			5·40	23·4
14.2-13	leucocratic granulite	0·512241	0·1330	−7·7	**1725**			8·70	39·0
27.1/31	metased.	0·511963	0·1176	−13·2	**1887**			10·0	52·0
12.1-21	metabasalt	0·512552	**0·1595**	−1·7	**1696**	1446	1·1	3·50	13·4
12.1-23	metabasalt	0·512183	0·1145	−8·9	**1494**			13·6	72·0
3.2/19	metarhyolite	0·513868	**0·3594**	24·0	**743**	1651	1·1	1·90	3·20
3.2/20	metabasalt	0·512498	0·1460	−2·7	**1481**			3·70	15·2
Moyes et al. *(1993), Antarctica, Dronning Maud Land, Sverdrupfjella*									
SF847	granitoids	0·51171	**0·172**	−18·1	**5190**	2941	1·1	108	381
SF8437		0·51153	0·084	−21·6	**1905**			22·7	162
SF85117		0·51142	0·083	−23·8	**2018**			36·2	263
SF8662		0·51132	0·064	−25·7	**1864**			175	1644
SF8663		0·51132	0·086	−25·7	**2182**			55·6	390
SF8666		0·51144	0·080	−23·4	**1950**			11·8	89·1
SF8665		0·51138	0·079	−24·5	**2003**			11·3	87·2
SF8696		0·51137	0·080	−24·7	**2029**			13·3	101
SF8698		0·51136	0·081	−24·9	**2056**			12·3	92·4
ABM89-38		0·51145	0·094	−23·2	**2164**			35·4	227
ABM89-40		0·51128	0·066	−26·5	**1930**			11·5	105
ABM89-32	xenoliths	0·51213	0·110	−9·9	**1507**			4·20	22·8
ABM89-33		0·51202	0·116	−12·1	**1768**			5·10	26·7
ABM89-34		0·51206	0·115	−11·3	**1690**			8·50	44·7
ABM89-35		0·51221	0·134	−8·3	**1805**			9·10	40·9
ABM89-36		0·51218	0·114	−8·9	**1491**			6·10	32·2
ABM89-37		0·51223	0·142	−8·0	**1962**			6·50	27·7
ABM89-39	hornfelses	0·51212	0·096	−10·1	**1342**			14·6	92·3
ABM89-41		0·51212	0·095	−10·1	**1331**			14·1	89·9

Table B1: continued

Sample	Rock type	$^{143}Nd/^{144}Nd$	$^{147}Sm/^{144}Nd$	ε_{Nd} T_0	$T_{DM}G$[a] (Ma)	Correct. $T_{DM}G$ (Ma)	Tcorr (Ga)	Sm (ppm)	Nd (ppm)
SF8537	paragneisses	0·51208	0·117	−10·9	**1693**			19·4	100
SF8539		0·51240	0·126	−4·6	**1315**			5·40	25·7
SF8564		0·51213	0·118	−9·9	**1632**			15·0	76·5
SF85126		0·51224	0·144	−7·8	**1997**			203	852
SF8642		0·51215	0·123	−9·5	**1688**			8·50	42·0
SLK5		0·51219	0·138	−8·7	**1939**			19·8	86·7
SLK10		0·51314	**0·206**	9·8	**382**	1039	1·1	2·30	6·90
Owada et al. *(1994), Antarctica, Enderby Land, Napier, Tonagh Island*									
21601G	mafic gneiss	0·511498	**0·1520**	−22·2	**4045**	3521	2·5	3·12	12·4
21602A	mafic gneiss	0·510977	0·1222	−32·4	**3594**			11·1	54·7
21602AB	mafic gneiss	0·511015	0·1279	−31·7	**3763**			12·7	59·9
21602AW	mafic gneiss	0·510660	0·1100	−38·6	**3632**			3·96	21·8
21602B	mafic gneiss	0·511805	0·1483	−16·2	**3121**			5·16	21·1
21602C	mafic gneiss	0·511585	0·1473	−20·5	**3569**			5·14	21·1
21603C	mafic gneiss	0·511109	0·1295	−29·8	**3667**			1·71	7·99
21603E	felsic gneiss	0·510609	0·1004	−39·6	**3396**			1·66	10·0
21603H	felsic gneiss	0·509972	0·0619	−52·0	**3172**			1·18	11·6
21603I	felsic gneiss	0·510128	0·0726	−49·0	**3244**			3·34	27·9
21603N	ultramafic gneiss	0·511576	**0·1614**	−20·7	**4537**	3643	2·5	1·50	5·63
21604G	ultramafic gneiss	0·510944	0·1302	−33·0	**3991**			1·61	7·45
Shiraishi & Kagami (1992), Antarctica, Sør–Rondane Mts									
8501-1503B	enderbitic gneisses	0·512560	0·1485	−1·5	**1394**			4·93	20·03
1503C		0·512620	**0·1554**	−0·4	**1403**	1120	0·65	3·14	12·19
1503D		0·512490	0·1376	−2·9	**1335**			2·73	12·00
1602D		0·512540	0·1491	−1·9	**1454**			3·44	13·94
902-2502A		0·512360	0·1145	−5·4	**1224**			2·37	12·50
2502B		0·512470	0·1370	−3·3	**1364**			3·31	14·60
8501-1601A	retrograde gneisses	0·512720	**0·1716**	1·6	**1579**	1070	0·65	1·22	4·28
1601C		0·512620	**0·1574**	−0·4	**1452**	1133	0·65	3·77	14·48
1602A		0·512550	0·1432	−1·7	**1312**			6·56	27·69
1602B		0·512530	0·1439	−2·1	**1368**			4·86	20·42
Shiraishi et al. *(1995), Antarctica, Lützow–Holm Bay, Cape Hinode*									
73123103	metatrondhjemites	0·512383	0·1281	−5·0	**1377**			1·67	7·86
74010107		0·512390	0·1267	−4·8	**1343**			2·39	11·4
73123116		0·512384	0·1255	−5·0	**1335**			1·18	5·70
74010606		0·512510	0·1498	−2·5	**1540**			3·60	14·5
74010701		0·512141	0·0928	−9·7	**1280**			0·90	5·84
73123106S		0·512173	0·0906	−9·1	**1218**			0·72	4·80
73123106K		0·512220	0·1059	−8·2	**1324**			1·00	5·72
74010105		0·511985	0·0679	−12·7	**1225**			0·23	2·06
74010115		0·512159	0·0956	−9·3	**1287**			0·52	3·30
74010113		0·512427	0·1306	−4·1	**1338**			2·51	11·6
74010304	metapelite	0·511943	0·1221	−13·6	**2012**			5·65	27·9

Sample	Rock type	$^{143}Nd/^{144}Nd$	$^{147}Sm/^{144}Nd$	ε_{Nd} T_0	$T_{DM}G$[a] (Ma)	Correct. $T_{DM}G$ (Ma)	Tcorr (Ga)	Sm (ppm)	Nd (ppm)
Tanaka et al. *(1985), Antarctica, Lützow–Holm Bay, Skarvsnes*									
C1	Grt granitoid	0·512400	0·1413	−4·6	**1590**			1·09	4·68
C4		0·512340	0·1320	−5·8	**1521**			14·23	65·2
C7		0·512290	0·1229	−6·8	**1453**			5·24	25·8
DePaolo et al. *(1982), Antarctica, Enderby Land*									
28-IV	2Px granulite	0·511654	**0·1533**	−19·2	**3748**	3307	2·5		15·57
28-II	Px granulite	0·510413	0·0909	−43·4	**3374**				8·41
28-III		0·510762	0·1112	−36·6	**3526**				1·46
28-VIII	Qtz–Fsp granulite	0·510992	0·1169	−32·1	**3376**				21·41
28-VI		0·510234	0·0782	−46·9	**3260**				4·70
28-VII		0·510229	0·0889	−47·0	**3542**				187·65
28-V	ironstone	0·510490	0·0864	−41·9	**3166**				16·52
Zhao et al. *(1995), Antarctica, Yamato–Belgica Complex*									
93286734	syenite	0·512167	0·11822	−9·2	**1577**			14·20	72·63
93286735	syenite	0·512155	0·09707	−9·4	**1309**			56·40	351·3
93286738	syenite	0·512176	0·12436	−9·0	**1669**			11·38	55·33
93286740	leuco-qtz syenite	0·512158	0·09044	−9·4	**1235**			39·76	265·8
93286744	syenite	0·512169	0·12152	−9·1	**1630**			10·74	53·43
93286753	mela-syenite	0·512172	0·12150	−9·1	**1625**			9·80	48·74
93286760	syenite	0·512103	0·11908	−10·4	**1693**			9·31	47·27
93286766	qtz-syenite	0·512147	0·12553	−9·6	**1741**			9·39	45·24
Y80A530	Opx-Bt gneiss	0·512101	0·10623	−10·5	**1495**			4·10	23·36

[a]Model age calculated after Goldstein *et al.* (1984). Calculation of Nd model ages in this study uses the following algorithm after Goldstein *et al.* (1984): $T_{DM} = 1/\lambda \ln (1 + \{[0{\cdot}51316 - (^{143}Nd/^{144}Nd)_{meas.}]/[0{\cdot}214 - (^{147}Sm/^{144}Nd)_{meas.}]\})$, where $\lambda = 6{\cdot}54 \times 10^{-12} yr^{-1}$ (DePaolo, 1988), 0·51316 is modern-day $^{143}Nd/^{144}Nd$ value of depleted mantle, 0·214 is $^{147}Sm/^{144}Nd$ value of DM in the model of Goldstein *et al.* (1984). Calculation of corrected Nd model ages uses the following algorithm [after Milisenda *et al.* (1988, 1994)]: $T_{DM} = 1/\lambda \ln [1 + (\{0{\cdot}51316 - (^{143}Nd/^{144}Nd)_{meas.} - [\exp(\lambda x T_{met}) - 1] \times (^{147}Sm/^{144}Nd)_{meas.} - 0{\cdot}12\})/(0{\cdot}214 - 0{\cdot}12]$, where T_{met} is time of metamorphism and change of parent/daughter ratio; 0·12 is average $^{147}Sm/^{144}Nd$ ratio of the continental crust (Taylor & McLennan, 1985). Corrected Nd model ages for samples with $^{147}Sm/^{144}Nd$ ratio higher than 0·15 are shown, but are not used for the histograms in Fig. 9.

[b]Not all nine analyses of the three rock samples in the micro-study of Burton & O'Nions (1990) have been used, because this would over-represent the regional abundance of the model ages.